Scheduling Divisible Workloads from Multiple Sources in Regular and Torus Mesh

A Dissertation Presented

by

Junwei Zhang

to

The Graduate School

in Partial Fulfillment of the

Requirements

for the Degree of

Doctor of Philosophy

in

Applied Mathematics and Statistics

Stony Brook University

August 2018

Stony Brook University

The Graduate School

Junwei Zhang

We, the dissertation committee for the above candidate for the
Doctor of Philosophy degree, hereby recommend
acceptance of this dissertation.

Thomas G. Robertazzi - Dissertation Advisor
Professor, Department of Electrical and Computer Engineering

Joseph S.B. Mitchell - Chairperson of Defense
Professor, Department of Applied Mathematics and Statistics

Esther M. Arkin - Member
Professor, Department of Applied Mathematics and Statistics

Yue Zhao - Member
Professor, Department of Electrical and Computer Engineering

This dissertation is accepted by the Graduate School.

Charles Taber
Dean of the Graduate School

Abstract of the Dissertation

Scheduling Divisible Workloads from Multiple Sources in Regular and Torus Mesh

by

Junwei Zhang

Doctor of Philosophy

in

Applied Mathematics and Statistics

Stony Brook University

2018

Abstract Here

Key Words:

To my Parents and all loving ones

Table of Contents

List of Figures

List of Tables

Acknowledgements

Chapter 1

Introduction

[?, ?]

Chapter 2

Closed-form Processor Equivalence

In large-scale data intensive problems with geographically distributed resources, load is generated from multiple sources[1]. It is assumed that the problem representation can be divided amongst the processors. Thus the problem representation is said to be "divisible". This chapter we discuss the closed-form processor equivalence[2][3] problem in the grid network of regular mesh, toroidal rectangle mesh.

This chapter is organized as follows. A problem introduction, notation and definitions are shown in Section I.

Section II considers about the unit core with front-end scenario. In the front-end situation, the regular mesh and torus rectangle mesh closed-form processor equivalence formula is investigated. Considering some various closed-form formula, the data injection position occurs on the corner processor, the boundary unit core or the inner grid processor.

Section III presents the unit core without front-end situation. In addition, the regular mesh and toroidal are discussed, respectively.

In section IV we give a comprehensive comparison result considering the different factors, for example the ratio between the communication ability to the computation capacity, the data injection position and the number of processors.

2.1 Problem Description

The processing of massive amounts of data on distributed and parallel networks is becoming more and more common. The problem of minimizing the processing time of extensive loads originating from a multiplicity of sources and being processed on a multiplicity of nodes presents a challenge.
The research user case involves the regular mesh Fig. 2.12 or toroidal mesh Fig. 2.2 of m*n processors. We refer to the $m * n$ processor as P_0, P_1, P_2, $\cdots$, P_{m*n-1}.

The workloads are denoted as $\mathbf{L_1}$, $\mathbf{L_2}$, $\cdots$, $\mathbf{L_k}$. We consider two situations, such as the processor contains the front-end and without front-end. In order to simply the question model, we have the following assumptions:

- We do not consider return communications.
- Communication delays are taken into consideration.
- The time costs of computation and communication are assumed to be linear function of the data size.
- The network environment is homogeneous, that is, all the processors have the same computation capacity.

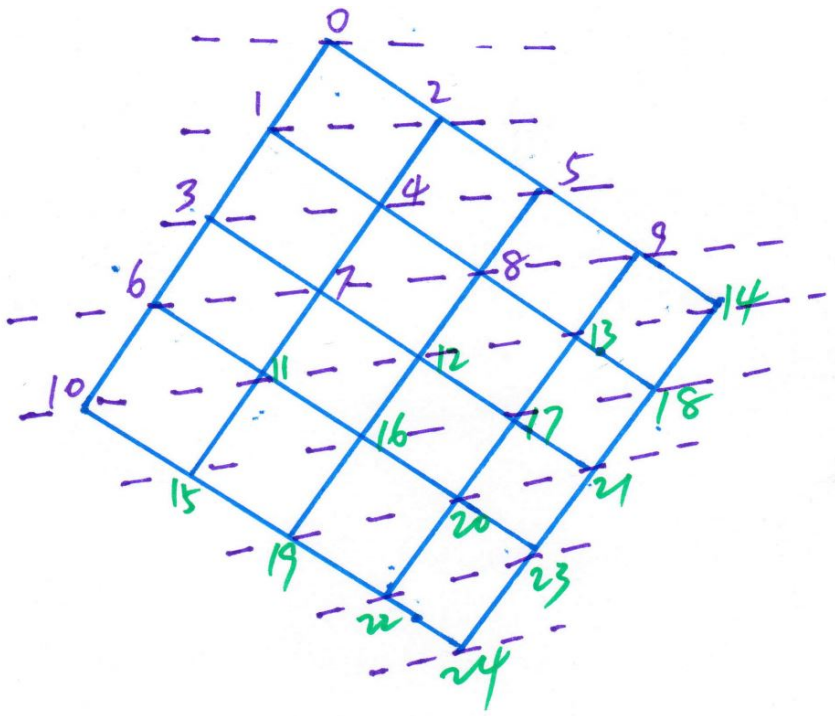

Figure 2.1: A m*n regular mesh(m = 5, n = 5)

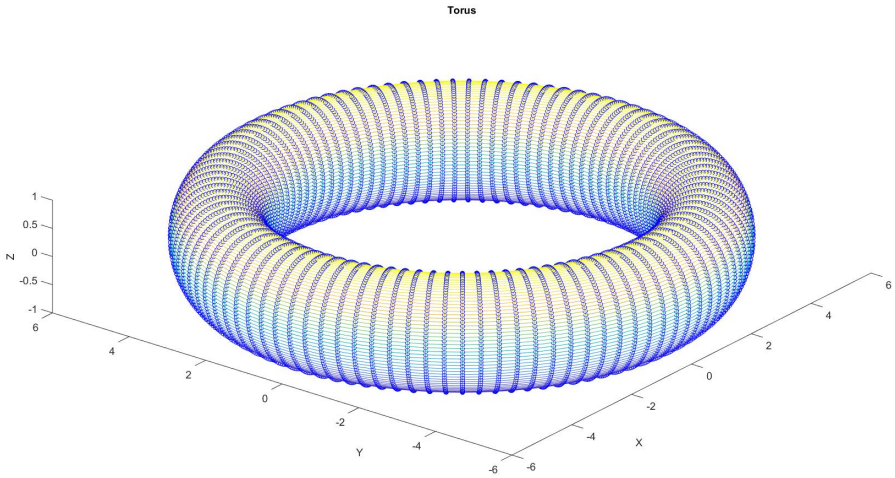

Figure 2.2: A toroidal mesh with grid unit cores

- The link speeds between any two unit cores are identical.
- The port of each processor is limited. In NOC(network on chip), the port number is 4 or5.
- The general graph's grid node's in-degree and out-degree is 4 or 5.

In the front-end assumption, the communication and the computation can be executed simultaneously. That is, upon receiving their respective load fractions, the processors start processing their own workload and rely all the other fractions to the next processor at the same time.

In the without front-end scenario, unlike the previous protocol, the processors now simultaneously receive the data and only start to process it as soon as each processor receives its entire load assignment[4].

Thus, the problem becomes how to partition and schedule the workloads amongst the processors to get the minimum finish time. This study will focus on the speedup metric which is defined as the ratio of computation time on one processor to the computation time on the entire $m * n$ processors.

To achieve the minimum solution is obtained by forcing the processors over a network to stop processing simultaneously. Intuitively, this is because the solution could be improved by transfer load from some busy processor to idle ones. The following notations and definitions are utilized:

Notations and Definitions

- D_i: The minimum number of hops from the node P_i to the nearest data load injection L.

- $level_i$:The Manhattan distance to the nearest data injection
- P_i: The ith processor. i should be from 0 to $m * n - 1$.
- L_i: The ith work load. i should be from 1 to k.
- α_0: The load fraction assigned to the root processor.
- α_i: The load fraction assigned to the ith processor.
- ω_i: The inverse computing speed on the ith processor.
- ω_{eq}: The inverse computing speed on an equivalent node collapsed from a regular mesh or toroidal.
- z_i: The inverse link speed on the ith link.
- T_{cp}: Computing intensity constant. The entire load can be processed in $\omega_i T_{cp}$ on the ith processor.
- T_{cm}: Communication intensity constant. The entire load can be transmitted in $z_i T_{cm}$ seconds over the ith link.
- $T_{f,n}$: The finish time of the whole regular network. Here $T_{f,n}$ is equal to $\omega_{eq} T_{cp}$.
- $T_{f,0}$: The finish time for the entire divisible load solved on the root processor. Here $T_{f,0}$ is equal to $1 \times \omega_0 T_{cp}$, that is $\omega_0 T_{cp}$.
- $\sigma = \frac{zT_{cm}}{\omega T_{cp}}$: The ratio between the communication speed to the computation speed, $0 < \sigma < 1$ [5] [6].

- $\sum_{i=1}^{k} L_i = 1$
- $\sum_{i=0}^{m*n-1} \alpha_i = 1$
- $Speedup = \frac{T_{f,0}}{T_{f,n}} = \frac{\omega T_{cp}}{\alpha_0 \omega T_{cp}} = \frac{1}{\alpha_0}$

2.2 With Front End Scenario

The processors compute and transfer the data load simultaneously. First we consider about the $2*2$ regular mesh, $2*n$ regular mesh. After, we analyze a more general case $m*n$ regular mesh and obtain a general closed-form matrix presentation. Finally, we give a key principle to address this type of question. In addition, different data injection position, such as the corner, boundary and inner grid point are also discussed.

2.2.1 Regular Mesh

Data Injection on The Corner Processor

2*2 Regular Mesh

The L_1 is assigned on the corner unit core P_0 Fig. 2.3. The whole task are tackled by four processors P_0, P_1, P_2, P_3 together.

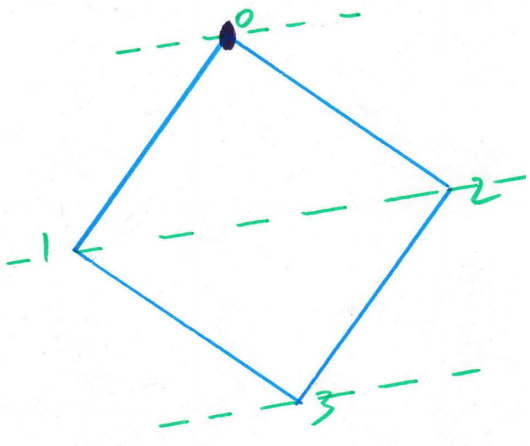

Figure 2.3: The 2*2 regular mesh and the data injection is on P_0

The processor P_0, P_1 and P_2 start to process its respective fraction at the same time. The port number of P_0 is limited, so the processor P_3 handles until the α_1 and α_2 are assigned completed to P_1 and P_2.

According to the divisible load theory[7], we can obtain the timing diagram Fig. 2.4.

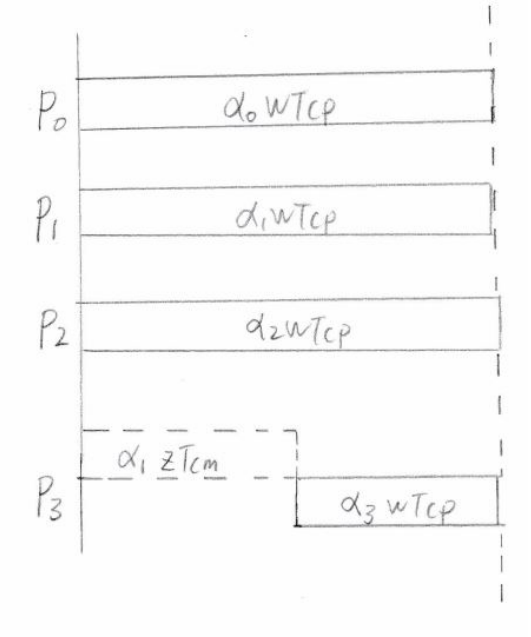

Figure 2.4: The timing diagram for 2*2 regular mesh and the data injection position is P_0

Based on the timing diagram, we can set the equations for the finish time of each processor to get ht optimal fragment size of loads:

$$
\begin{cases}
\alpha_0 \omega T_{cp} = T_{f,m} & (2.1) \\
\alpha_0 \omega T_{cp} = T_{f,m} & (2.2) \\
\alpha_1 \omega T_{cp} = T_{f,m} & (2.3) \\
\alpha_2 \omega T_{cp} = T_{f,m} & (2.4) \\
\alpha_1 z T_{cm} + \alpha_3 \omega T_{cp} = T_{f,m} & (2.5) \\
\alpha_0 + \alpha_1 + \alpha_2 + \alpha_3 = 1 & (2.6) \\
\sigma = \dfrac{z T_{cm}}{\omega T_{cp}} & (2.7) \\
0 < \sigma < 1 & (2.8) \\
0 < \alpha_0 \leq 1 & (2.9) \\
0 \leq \alpha_1, \alpha_2, \alpha_3 < 1 & (2.10)
\end{cases}
$$

We can obtain the

$$\alpha_1 = \alpha_2$$

The group of equations are represented by the matrix form:

$$
\begin{bmatrix} 1 & 2 & 1 \\ 1 & -1 & 0 \\ 0 & \sigma - 1 & 1 \end{bmatrix} \times \begin{bmatrix} \alpha_0 \\ \alpha_1 \\ \alpha_3 \end{bmatrix} = \begin{bmatrix} 1 \\ 0 \\ 0 \end{bmatrix} \tag{2.11}
$$

The simulation result is illustrated:

In Fig. 2.5, P_0, P_1, P_2 three processors have the same data fraction workload, so the curve of α_0 and α_1 coincide. The figure says that the σ value

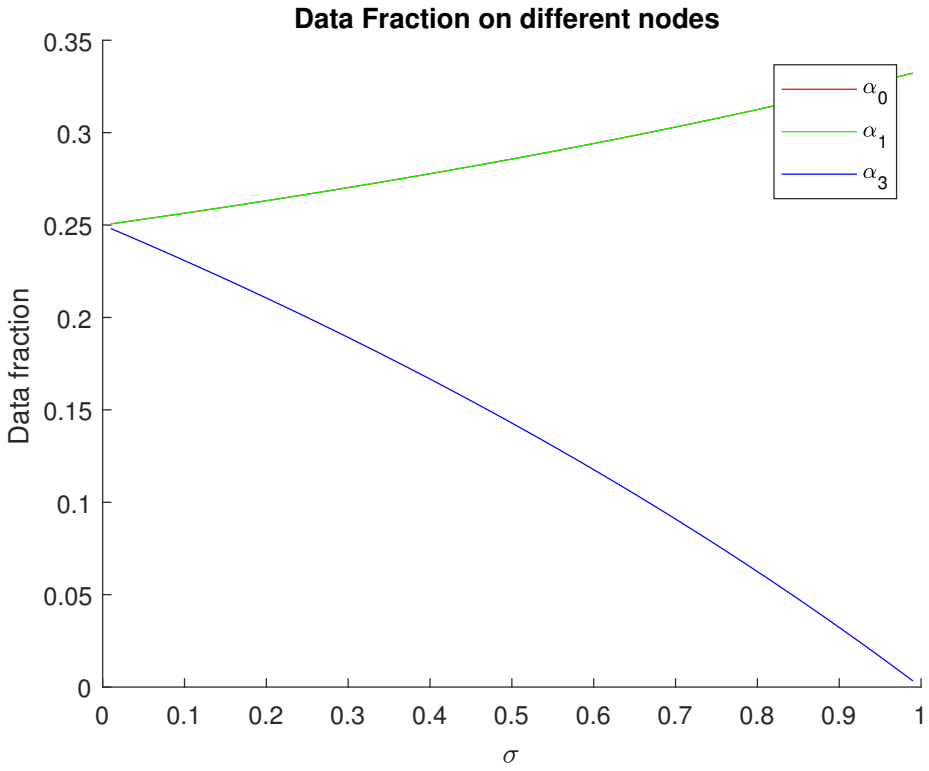

Figure 2.5: 2*2 regular mesh. α_0, α_1, α_2, α_3 value

grows and the α_3 drops simultaneously. In other words, the communication capacity drops down and there is less data workload assigned to P_3. Further, it means it will be economical to keep the load local nor distribute to other processor.

The speedup is:

$$Speedup = \frac{T_{f,0}}{T_{f,n}} = \frac{\omega T_{cp}}{\alpha_0 \omega T_{cp}} = \frac{1}{\alpha_0}$$

2*3 Regular Mesh

In the $2*3$ Fig. 2.6 regular mesh, L_1 happens on processor P_0. There are 6 processors to take the responsibility.

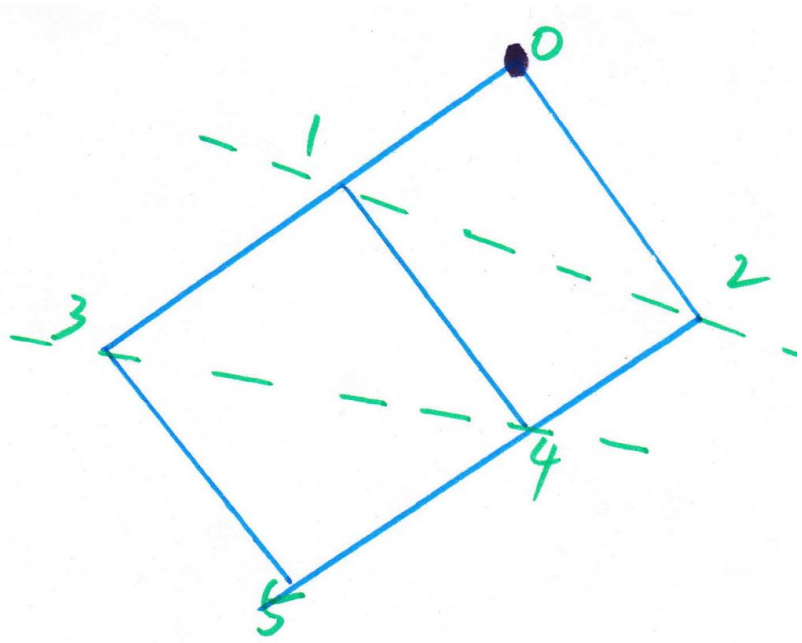

Figure 2.6: The 2*3 regular mesh and the data injection happens on corner processor P_0

P_0, P_1 and P_2 start processing the load at the same time. According the processor P_3 and P_4 start to work until they get the data from their parent processor P_1, P_2. Yet, the number of port of each processor is 4 or 5. So the fraction of α_3, α_4 are queued in the L_1. So the P_3 and P_4 have to wait the fraction of α_1 and α_2 are transmitted completely and then they will obtain their respective workload task fraction.

The last unit core P_5 starts to execute until the work load fraction α_0, α_1, α_2,

α_3, α_4 are transmitted completed.

According to the divisible load theory[7], we can obtain the timing diagram Fig. 2.7.

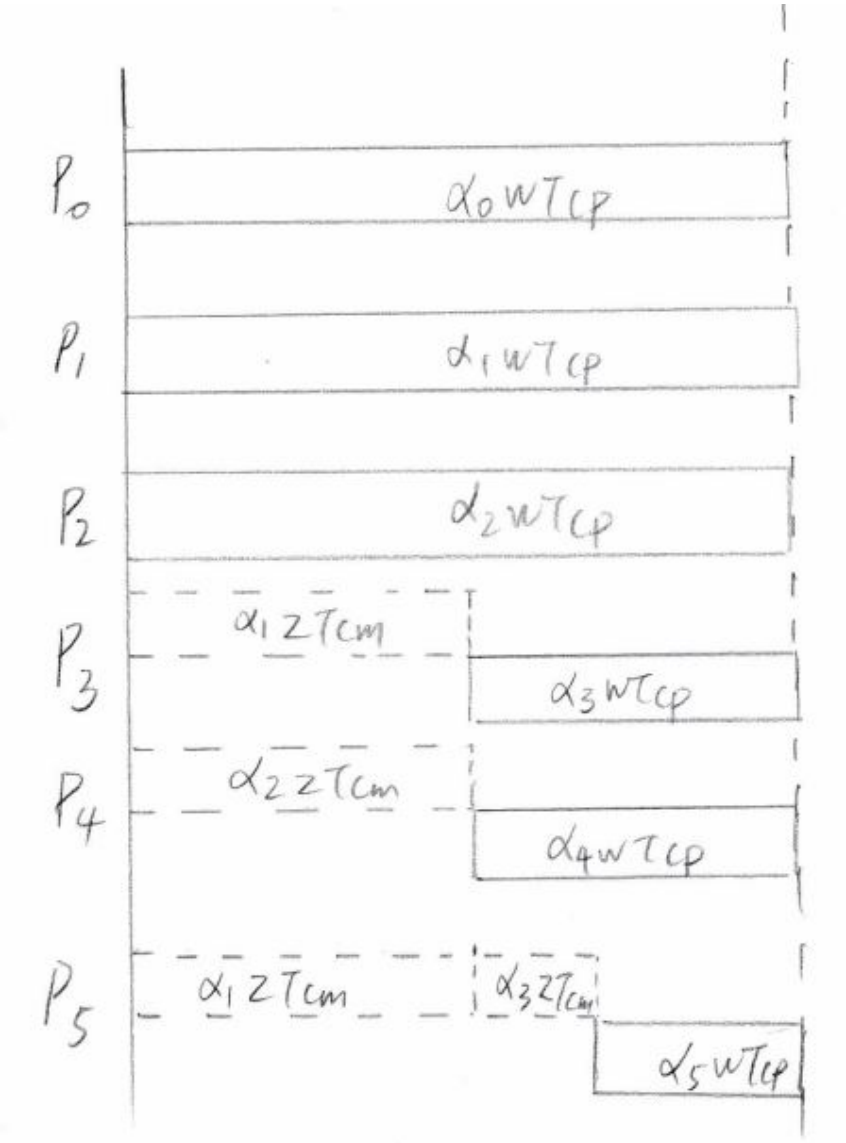

Figure 2.7: The timing diagram for a 2*3 regular mesh and the data injection happens on processor P_0

The equations as follows:

$$
\begin{cases}
\alpha_0 \omega T_{cp} = T_{f,m} & (2.12) \\
\alpha_1 \omega T_{cp} = T_{f,m} & (2.13) \\
\alpha_2 \omega T_{cp} = T_{f,m} & (2.14) \\
\alpha_1 z T_{cm} + \alpha_3 \omega T_{cp} = T_{f,m} & (2.15) \\
\alpha_2 z T_{cm} + \alpha_4 \omega T_{cp} = T_{f,m} & (2.16) \\
(\alpha_1 + \alpha_3) z T_{cm} + \alpha_5 \omega T_{cp} = T_{f,m} & (2.17) \\
\alpha_0 + \alpha_1 + \alpha_2 + \alpha_3 + \alpha_4 + \alpha_5 = 1 & (2.18) \\
\sigma = \dfrac{z T_{cm}}{\omega T_{cp}} & (2.19) \\
0 < \sigma < 1 & (2.20) \\
0 < \alpha_0 \leq 1 & (2.21) \\
0 \leq \alpha_1, \alpha_2, \alpha_3, \alpha_4, \alpha_5 < 1 & (2.22)
\end{cases}
$$

After the simplification, we found:

$$
\begin{cases}
\alpha_1 = \alpha_2 & (2.23) \\
\alpha_3 = \alpha_4 & (2.24)
\end{cases}
$$

The matrix closed-form formula is:

$$\begin{bmatrix} 1 & 2 & 2 & 1 \\ 1 & -1 & 0 & 0 \\ 0 & \sigma-1 & 1 & 0 \\ 0 & \sigma-1 & \sigma & 1 \end{bmatrix} \times \begin{bmatrix} \alpha_0 \\ \alpha_1 \\ \alpha_3 \\ \alpha_5 \end{bmatrix} = \begin{bmatrix} 1 \\ 0 \\ 0 \\ 0 \end{bmatrix} \tag{2.25}$$

The simulation result are shown in Fig. 2.8. P_0, P_1 have the same fraction so their curves of α_0 and α_1 coincide.

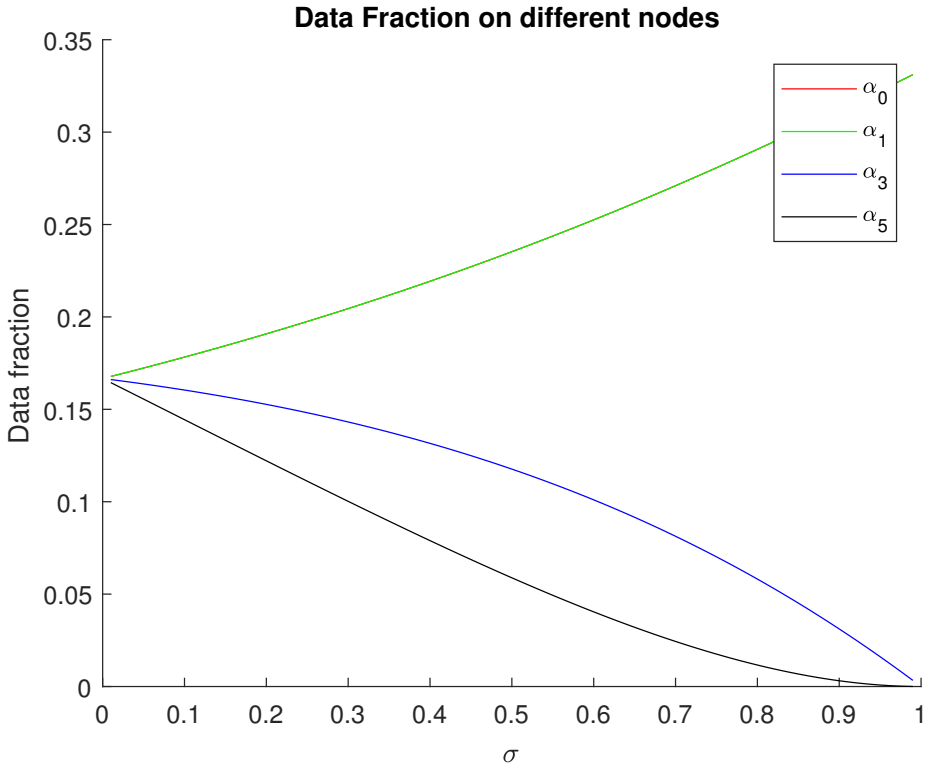

Figure 2.8: 2*2 regular mesh. α_0, α_1, α_3, α_5 data fraction value

2*n Regular Mesh

The $2*n$ Fig. 2.9 homogeneous regular mesh address L_1 at the same time and L_1 happens on P_0.

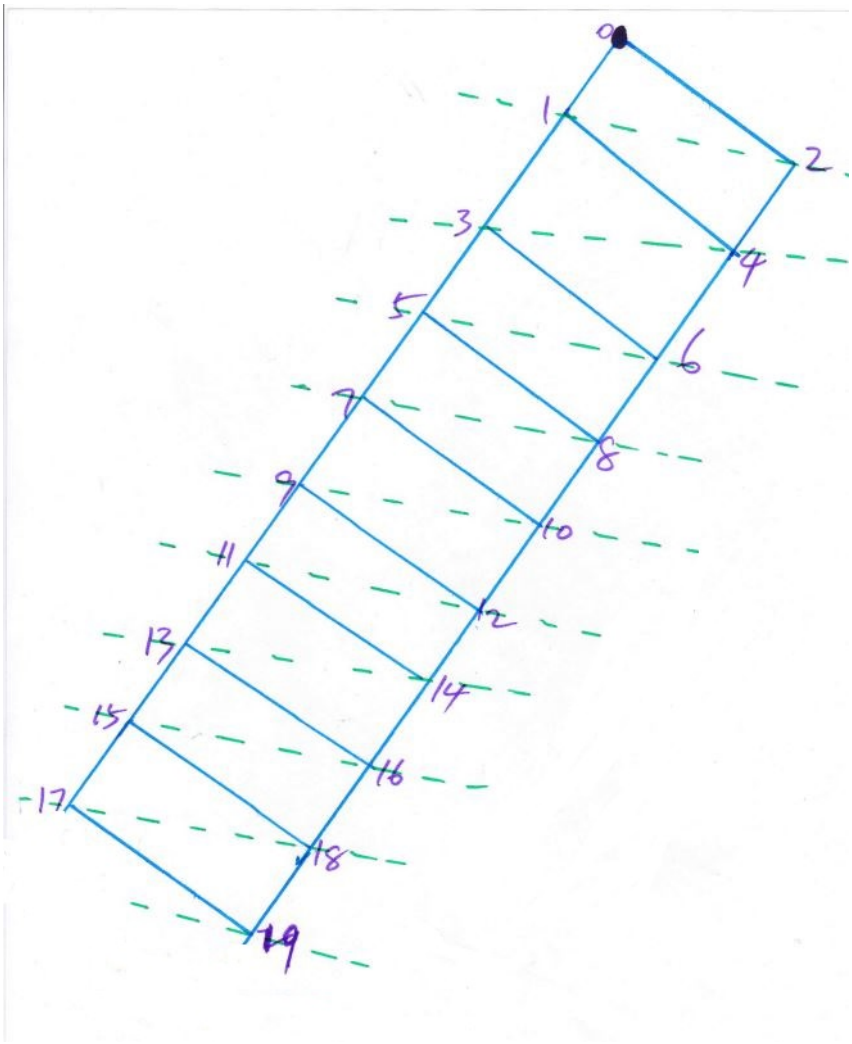

Figure 2.9: The 2*n (n = 10) regular mesh and the workload happens on P_0

Similarly to the analysis of Fig. 2.4 and Fig. 2.7, the timing diagram for Fig. 2.9 is shown in Fig. 2.10

The equations are presented as:

$$
\begin{cases}
\alpha_0 \omega T_{cp} = T_{f,m} & (2.26) \\
\alpha_1 \omega T_{cp} = T_{f,m} & (2.27) \\
\alpha_2 \omega T_{cp} = T_{f,m} & (2.28) \\
\alpha_1 z T_{cm} + \alpha_3 \omega T_{cp} = T_{f,m} & (2.29) \\
\alpha_2 z T_{cm} + \alpha_4 \omega T_{cp} = T_{f,m} & (2.30) \\
(\alpha_1 + \alpha_3) z T_{cm} + \alpha_5 \omega T_{cp} = T_{f,m} & (2.31) \\
\vdots & (2.32) \\
(\alpha_1 + \alpha_3 + \cdots + \alpha_{2\times n-1}) z T_{cm} + \alpha_{2\times n-1} \omega T_{cp} = T_{f,m} & (2.33) \\
\alpha_0 + \cdots + \alpha_{2\times n-1} = 1 & (2.34) \\
\sigma = \dfrac{z T_{cm}}{\omega T_{cp}} & (2.35) \\
0 < \sigma < 1 & (2.36) \\
0 < \alpha_0 \quad \alpha_1 \quad \alpha_3 \quad \cdots \quad \alpha_{2\times n-1} < 1 & (2.37) \\
& (2.38)
\end{cases}
$$

The matrix closed-form is shown:

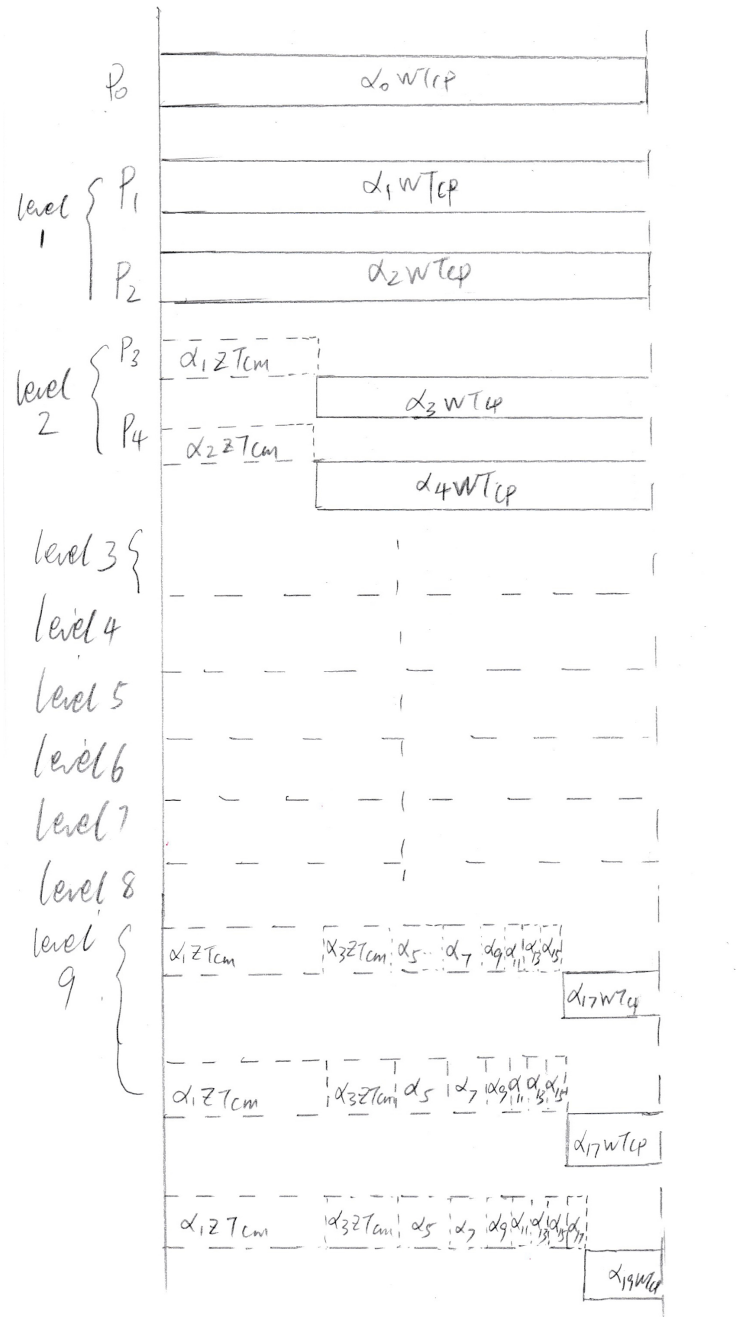

Figure 2.10: The timing diagram for 2*10 regular mesh and the data injection happens on P_0

$$\begin{bmatrix} 1 & 2 & 2 & \cdots & 2 & 2 & 1 \\ 1 & -1 & 0 & \cdots & 0 & 0 & 0 \\ 0 & \sigma-1 & 1 & \cdots & 0 & 0 & 0 \\ 0 & \sigma-1 & \sigma & 1 & 0 & \cdots & 0 \\ 0 & \sigma-1 & \sigma & \sigma & 1 & 0 & 0 \\ \vdots & \vdots & \vdots & \vdots & \ddots & \ddots & \\ 0 & \sigma-1 & \sigma & \cdots & \sigma & \sigma & 1 \end{bmatrix} \times \begin{bmatrix} \alpha_0 \\ \alpha_1 \\ \alpha_3 \\ \alpha_5 \\ \vdots \\ \alpha_{2\times n-3} \\ \alpha_{2\times n-1} \end{bmatrix} = \begin{bmatrix} 1 \\ 0 \\ 0 \\ 0 \\ 0 \\ 0 \\ \vdots \\ 0 \\ 0 \end{bmatrix} \tag{2.39}$$

Finally, the speedup is:

$$Speedup = \frac{T_{f,0}}{T_{f,n}} = \frac{\omega T_{cp}}{\alpha_0 \omega T_{cp}} = \frac{1}{\alpha_0}$$

After three user cases' investigation, we find a crucial rule:

$$\forall D_i = D_j, \quad then \quad \alpha_i = \alpha_j, \quad 0 \leq i, j \leq m * n - 1$$

m*n Regular Mesh

Considering a general $m * n$ regular mesh, such as Fig. 2.11 Fig. 2.12.

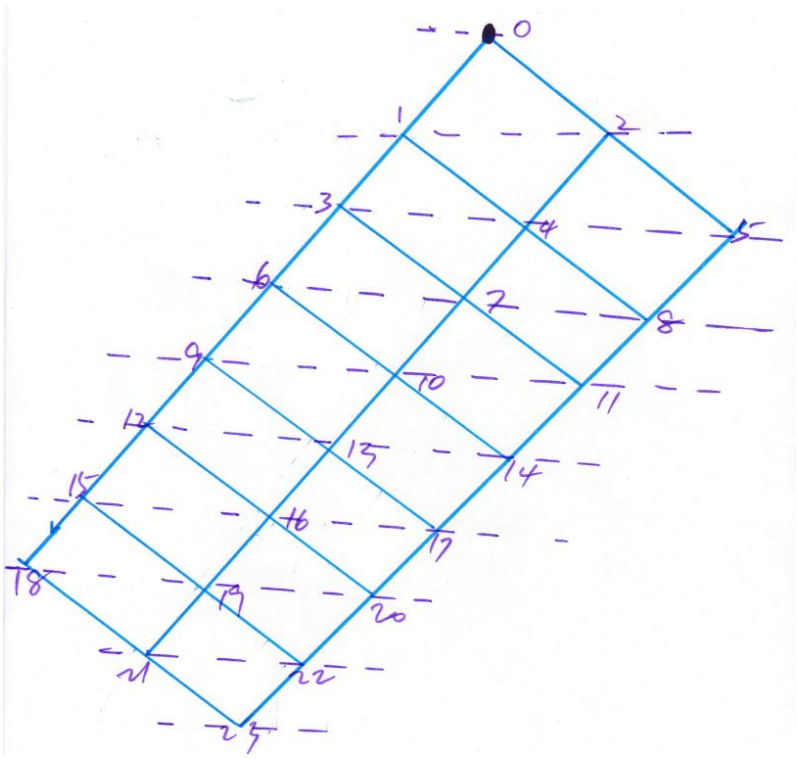

Figure 2.11: 3*8 regular mesh. The data injection position is P_0

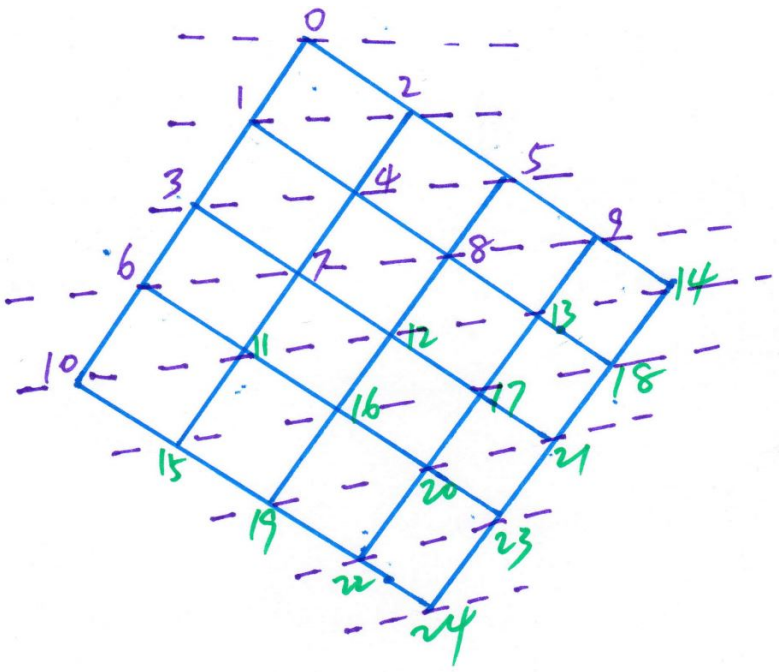

Figure 2.12: 5*5 regular mesh. The data injection position is processor P_0

Utilizing the rule, we obtain the closed-form matrix equations for Fig. 2.11:

$$\begin{bmatrix} 1 & 2 & 3 & 3 & 3 & 3 & 3 & 3 & 2 & 1 \\ 1 & -1 & 0 & 0 & 0 & 0 & 0 & 0 & 0 & 0 \\ 0 & \sigma-1 & 1 & 0 & 0 & 0 & 0 & 0 & 0 & 0 \\ 0 & \sigma-1 & \sigma & 1 & 0 & 0 & 0 & 0 & 0 & 0 \\ 0 & \sigma-1 & \sigma & \sigma & 1 & 0 & 0 & 0 & 0 & 0 \\ 0 & \sigma-1 & \sigma & \sigma & \sigma & 1 & 0 & 0 & 0 & 0 \\ 0 & \sigma-1 & \sigma & \sigma & \sigma & \sigma & 1 & 0 & 0 & 0 \\ 0 & \sigma-1 & \sigma & \sigma & \sigma & \sigma & \sigma & 1 & 0 & 0 \\ 0 & \sigma-1 & \sigma & \sigma & \sigma & \sigma & \sigma & \sigma & 1 & 0 \\ 0 & \sigma-1 & \sigma & \sigma & \sigma & \sigma & \sigma & \sigma & \sigma & 1 \end{bmatrix} \times \begin{bmatrix} \alpha_0 \\ \alpha_1 \\ \alpha_3 \\ \alpha_6 \\ \alpha_9 \\ \alpha_{12} \\ \alpha_{15} \\ \alpha_{18} \\ \alpha_{21} \\ \alpha_{23} \end{bmatrix} = \begin{bmatrix} 1 \\ 0 \\ 0 \\ 0 \\ 0 \\ 0 \\ 0 \\ 0 \\ \vdots \\ 0 \end{bmatrix} \tag{2.40}$$

Also, the matrix equation for Fig. 2.12:

$$\begin{bmatrix} 1 & 2 & 3 & 4 & 5 & 4 & 3 & 2 & 1 \\ 1 & -1 & 0 & 0 & 0 & 0 & 0 & 0 & 0 \\ 0 & \sigma-1 & 1 & 0 & 0 & 0 & 0 & 0 & 0 \\ 0 & \sigma-1 & \sigma & 1 & 0 & 0 & 0 & 0 & 0 \\ 0 & \sigma-1 & \sigma & \sigma & 1 & 0 & 0 & 0 & 0 \\ 0 & \sigma-1 & \sigma & \sigma & \sigma & 1 & 0 & 0 & 0 \\ 0 & \sigma-1 & \sigma & \sigma & \sigma & \sigma & 1 & 0 & 0 \\ 0 & \sigma-1 & \sigma & \sigma & \sigma & \sigma & \sigma & 1 & 0 \\ 0 & \sigma-1 & \sigma & \sigma & \sigma & \sigma & \sigma & \sigma & 1 \end{bmatrix} \times \begin{bmatrix} \alpha_0 \\ \alpha_1 \\ \alpha_3 \\ \alpha_6 \\ \alpha_{10} \\ \alpha_{15} \\ \alpha_{19} \\ \alpha_{22} \\ \alpha_{24} \end{bmatrix} = \begin{bmatrix} 1 \\ 0 \\ 0 \\ 0 \\ 0 \\ 0 \\ 0 \\ \vdots \\ 0 \end{bmatrix} \tag{2.41}$$

Data Injection On the Boundary Processor

After explain the corner scenario, we extend the rule to boundary processor condition.

If the single data injection roots on the boundary processor, for example Fig. 2.13.

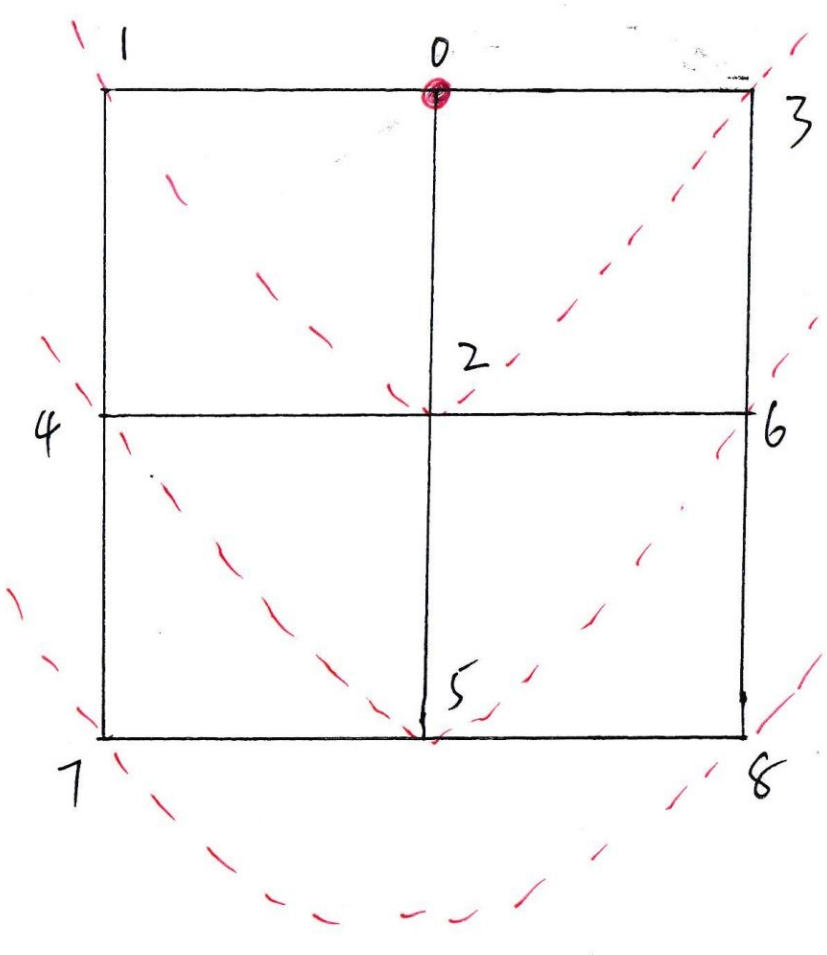

Figure 2.13: The 3*3 regular mesh and the data injection position is P_0

The timing diagram is Fig. 2.14:

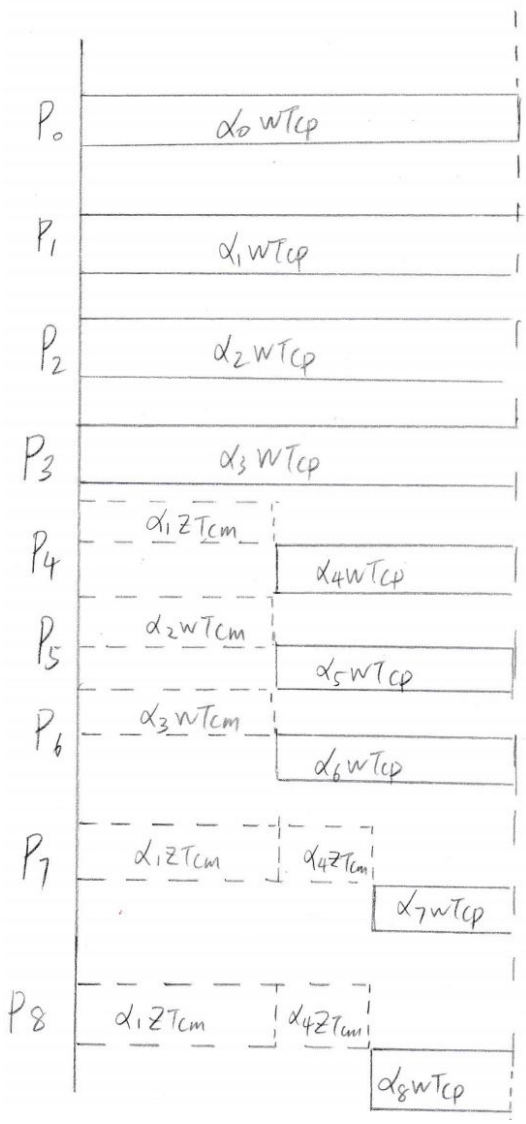

Figure 2.14: The timing diagram for 3*3 regular mesh and the data injection occurs on the boundary processor P_0

The equations are:

$$
\begin{cases}
\alpha_0 \omega T_{cp} = T_{f,m} & (2.42)\\
\alpha_1 \omega T_{cp} = T_{f,m} & (2.43)\\
\alpha_2 \omega T_{cp} = T_{f,m} & (2.44)\\
\alpha_3 \omega T_{cp} = T_{f,m} & (2.45)\\
\alpha_1 z T_{cm} + \alpha_4 \omega T_{cp} = T_{f,m} & (2.46)\\
\alpha_2 z T_{cm} + \alpha_5 \omega T_{cp} = T_{f,m} & (2.47)\\
\alpha_3 z T_{cm} + \alpha_6 \omega T_{cp} = T_{f,m} & (2.48)\\
(\alpha_1 + \alpha_4) z T_{cm} + \alpha_7 \omega T_{cp} = T_{f,m} & (2.49)\\
(\alpha_2 + \alpha_5) z T_{cm} + \alpha_8 \omega T_{cp} = T_{f,m} & (2.50)\\
\alpha_0 + \cdots + \alpha_8 = 1 & (2.51)\\
\sigma = \dfrac{z T_{cm}}{\omega T_{cp}} & (2.52)\\
0 < \sigma < 1 & (2.53)\\
0 < \alpha_0 \quad \alpha_1 \quad \alpha_2 \quad \cdots \quad \alpha_8 < 1 & (2.54)\\
& (2.55)
\end{cases}
$$

And the matrix form is :

$$\begin{bmatrix} 1 & 3 & 3 & 2 \\ 1 & -1 & 0 & 0 \\ 0 & \sigma-1 & 1 & 0 \\ 0 & \sigma-1 & \sigma & 1 \end{bmatrix} \times \begin{bmatrix} \alpha_0 \\ \alpha_1 \\ \alpha_4 \\ \alpha_7 \end{bmatrix} = \begin{bmatrix} 1 \\ 0 \\ 0 \\ 0 \end{bmatrix} \tag{2.56}$$

And the simulation result is shown: P_0 and P_1 have the same α, so the curve of α_0 and α_1 coincide.

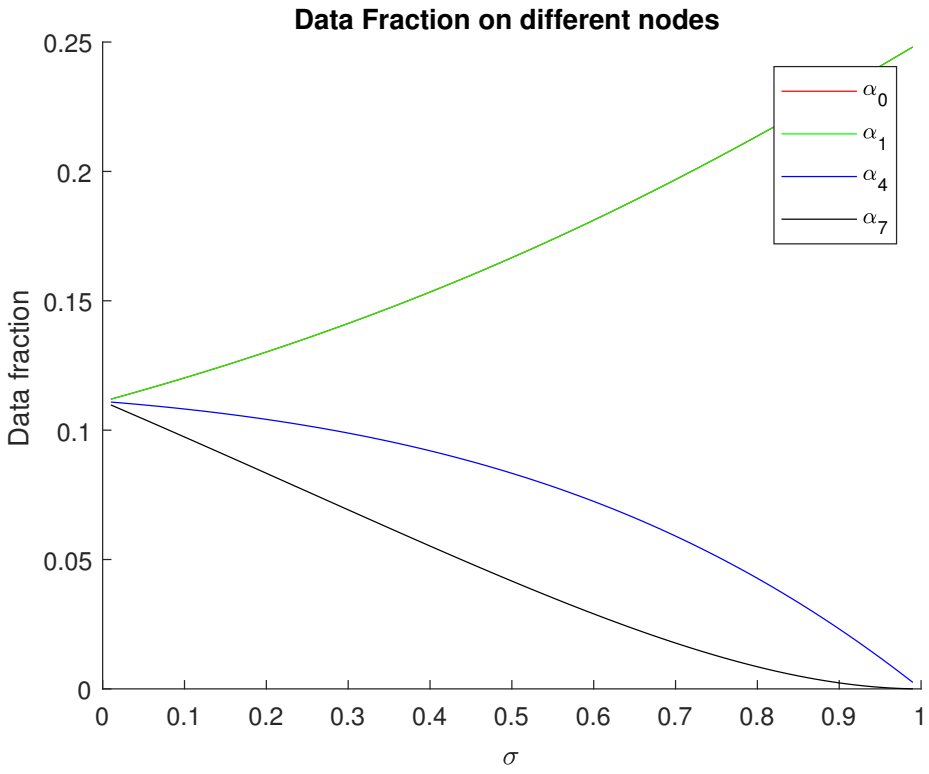

Figure 2.15: The data fraction simulation result of 3*3 regular mesh and the data injection happens on the boundary P_0

Data Injection On The Inner Grid Processor

L_1 is on the inner grid processor P_0Fig. 2.16,

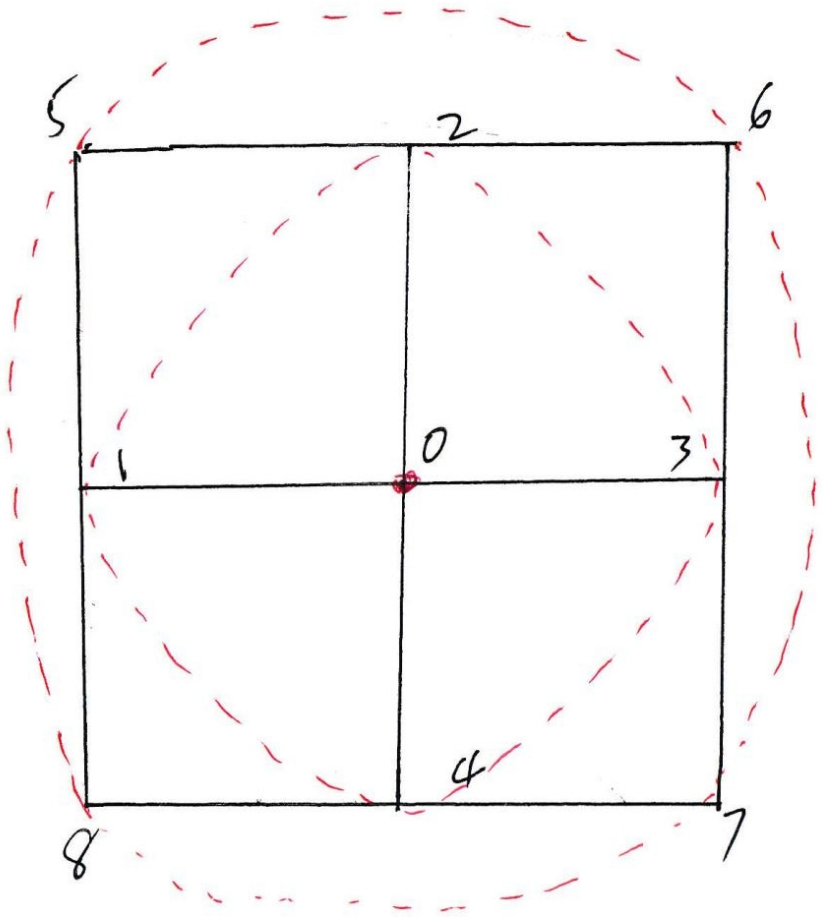

Figure 2.16: 3*3 regular mesh. The data injection position is inner grid point P_0

The timing diagram for this user case is illustrated as Fig. 2.17:

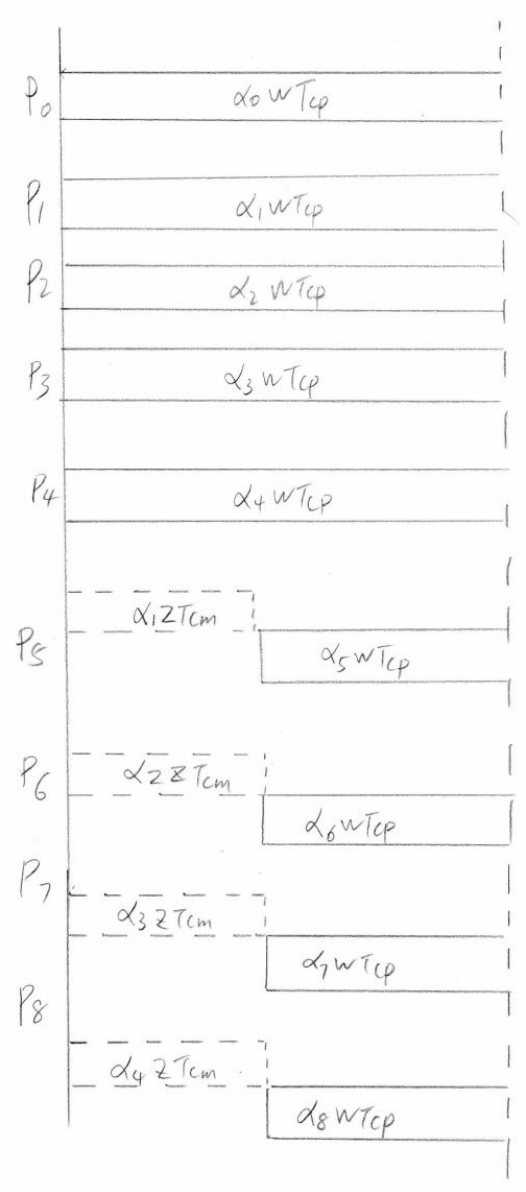

Figure 2.17: The timing diagram for 3*3 regular mesh and the data injection is inner grid P_0

The group of equations are:

$$
\begin{cases}
\alpha_0 \omega T_{cp} = T_{f,m} & (2.57)\\
\alpha_1 \omega T_{cp} = T_{f,m} & (2.58)\\
\alpha_2 \omega T_{cp} = T_{f,m} & (2.59)\\
\alpha_3 \omega T_{cp} = T_{f,m} & (2.60)\\
\alpha_4 \omega T_{cp} = T_{f,m} & (2.61)\\
\alpha_1 z T_{cm} + \alpha_5 \omega T_{cp} = T_{f,m} & (2.62)\\
\alpha_1 z T_{cm} + \alpha_6 \omega T_{cp} = T_{f,m} & (2.63)\\
\alpha_1 z T_{cm} + \alpha_7 \omega T_{cp} = T_{f,m} & (2.64)\\
\alpha_1 z T_{cm} + \alpha_8 \omega T_{cp} = T_{f,m} & (2.65)\\
\sigma = \dfrac{z T_{cm}}{\omega T_{cp}} & (2.66)\\
0 < \sigma < 1 & (2.67)\\
0 < \alpha_0 \quad \alpha_1 \quad \alpha_2 \quad \cdots \quad \alpha_8 < 1 & (2.68)
\end{cases}
$$

The matrix form is :

$$
\begin{bmatrix} 1 & 4 & 4 \\ 1 & -1 & 0 \\ 0 & \sigma - 1 & 1 \end{bmatrix} \times \begin{bmatrix} \alpha_0 \\ \alpha_1 \\ \alpha_5 \end{bmatrix} = \begin{bmatrix} 1 \\ 0 \\ 0 \end{bmatrix} \tag{2.69}
$$

The simulation result for the inner grid is Fig. 2.18: P_0 and P_1 have the same α value, so the curve of α_0 and α_1 coincide.

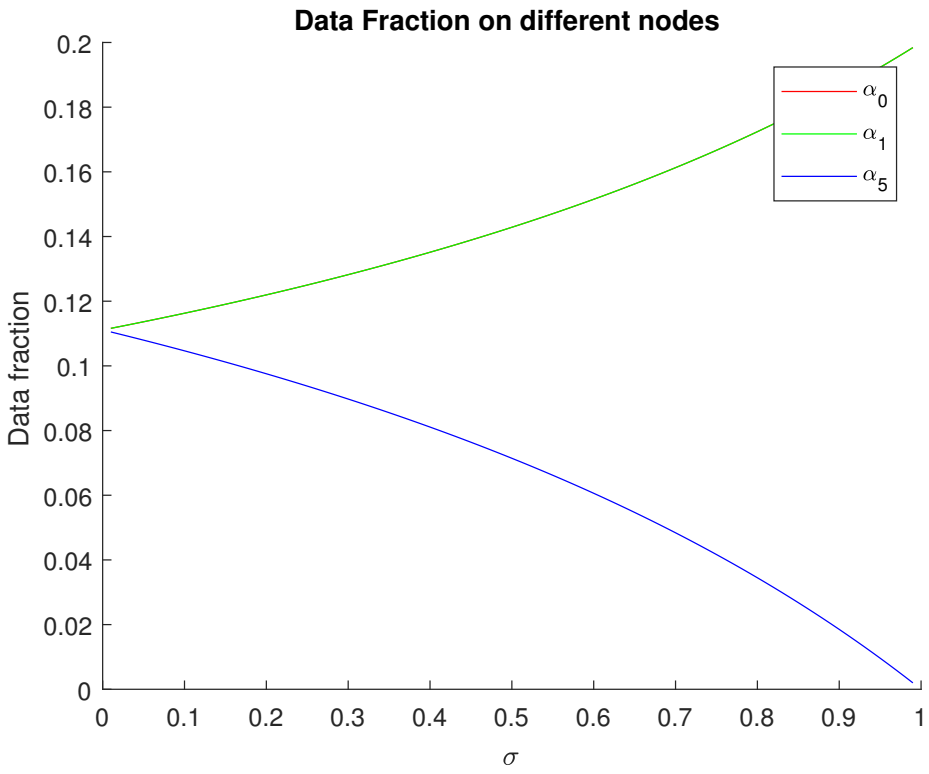

Figure 2.18: 3*3 regular mesh. The data injection position is inner grid point P_0

2.2.2 Torus mesh

According to the paper[8], there are three different torus mesh. In this paper, out intent is not to propose one model to "fit all" problems but rather to indicate one normal case. Other situation can be extend use the same rule. The toroidal network is also a regular complex in that each polygonal face has the same number of links and each node is connected to the same number of links.

We consider the toroidal network is Fig. 2.19 and Fig. 2.20.

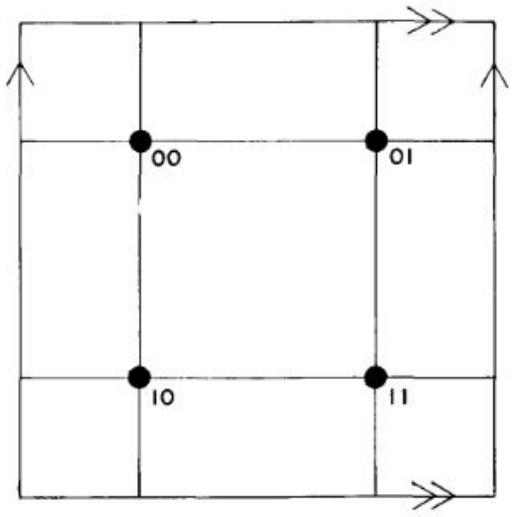

Figure 2.19: The rectangular toroidal network

Based on the rule, this question is transfered to that given a D_i and I find the number of instance.

- We assume the toroidal processor number is $m * n$, in other words, the width is m and the height is n.
- L to present the load injection.

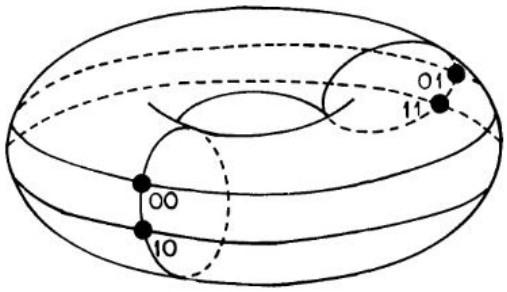

Figure 2.20: The rectangular toroidal network

- L_x is the L's X coordinate.
- L_y is the L's Y coordinate.
- D_i to present the shortest Manhattan distance between the grid node i and L.
- D_x is the X coordinate shortest Manhattan distance.
- D_y is the Y coordinate shortest Manhattan distance.
- N_x is the node i's X coordinate.
- N_y is the node i's Y coordinate.

$$\begin{cases} D = D_x + D_y & (2.70) \\ D_x = \min\{\|N_x - L_x\|, m - \|N_x - L_x\|\} & (2.71) \\ D_y = \min\{\|N_y - L_y\|, n - \|N_y - L_y\|\} & (2.72) \end{cases}$$

In the $m*n(m=6,n=6)$ toroidal networks, L happens on grid position $(4,2)$. We calculate the D_i matrix Table 2.1 by breadth first search(***BFS***) algorithm.

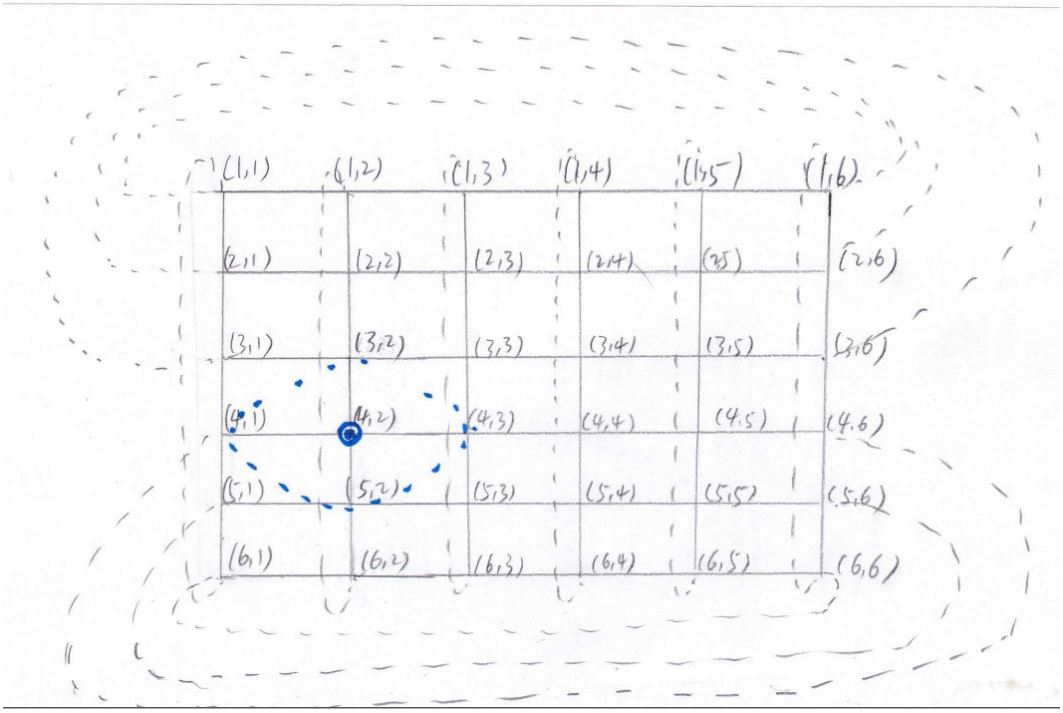

Figure 2.21: The m*n toroidal network and the data injection is $P_{4,2}$

D_i	Number
0	1
1	4
2	8
3	10
4	8
5	4
6	1

Table 2.1: The processor number of various D_i

And the D_i matrix as follow in table Table 2.1

The matrix closed-form is

$$\begin{bmatrix} 1 & 4 & 8 & 10 & 8 & 4 & 1 \\ 1 & -1 & 0 & 0 & 0 & 0 & 0 \\ 0 & \sigma-1 & 1 & 0 & 0 & 0 & 0 \\ 0 & \sigma-1 & \sigma & 1 & 0 & 0 & 0 \\ 0 & \sigma-1 & \sigma & \sigma & 1 & 0 & 0 \\ 0 & \sigma-1 & \sigma & \sigma & \sigma & 1 & 0 \\ 0 & \sigma-1 & \sigma & \sigma & \sigma & \sigma & 1 \end{bmatrix} \times \begin{bmatrix} \alpha_0 \\ \alpha_1 \\ \alpha_2 \\ \alpha_3 \\ \alpha_4 \\ \alpha_5 \\ \alpha_6 \end{bmatrix} = \begin{bmatrix} 1 \\ 0 \\ 0 \\ 0 \\ 0 \\ 0 \\ 0 \end{bmatrix} \tag{2.73}$$

The simulation result is :

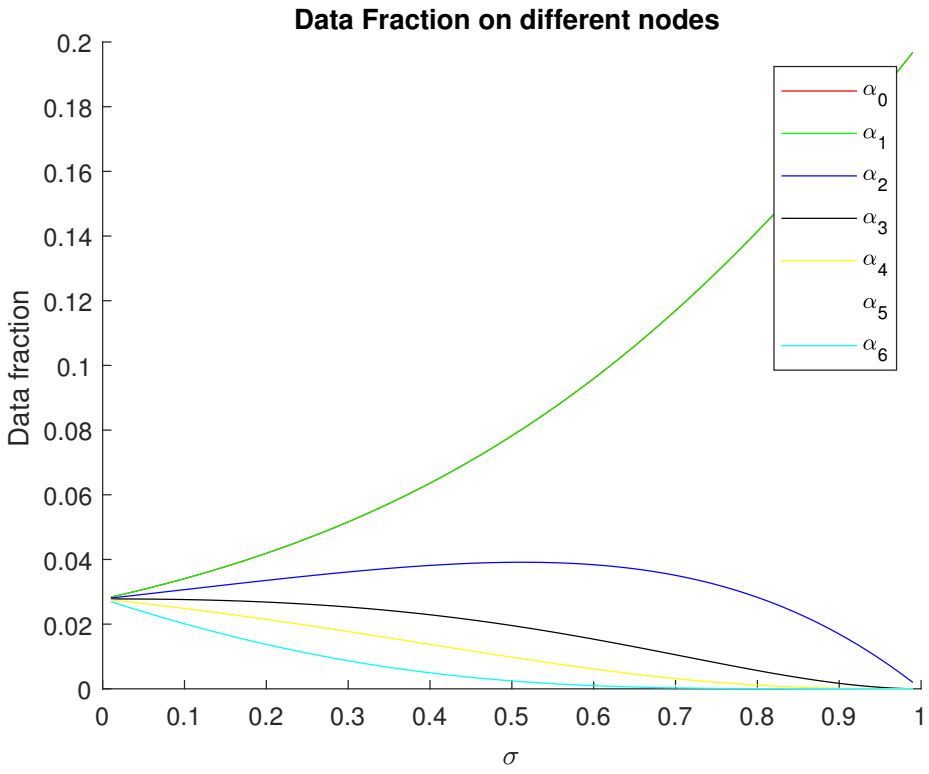

Figure 2.22: The data fraction deployed based on the radius value

From Fig. 2.22, we see as the σ value grows, more and more workload are assigned to the $P_{4,2}$ and its one hop neighbors. That is, as the communication ability goes down, the economical method is to process the data locally.

2.2.3 General Case

$$\begin{bmatrix} 1 & m_1 & m_2 & \cdots & m_{n-2} & m_{n-1} & m_n \\ 1 & -1 & 0 & \cdots & 0 & 0 & 0 \\ 0 & \sigma-1 & 1 & \cdots & 0 & 0 & 0 \\ 0 & \sigma-1 & \sigma & 1 & 0 & \cdots & 0 \\ 0 & \sigma-1 & \sigma & \sigma & 1 & 0 & 0 \\ \vdots & \vdots & \vdots & \vdots & \ddots & \ddots & \\ 0 & \sigma-1 & \sigma & \cdots & \sigma & \sigma & 1 \end{bmatrix} \times \begin{bmatrix} \alpha_{l_0} \\ \alpha_{l_1} \\ \alpha_{l_2} \\ \alpha_{l_3} \\ \vdots \\ \alpha_{l_{n-1}} \\ \alpha_{l_n} \end{bmatrix} = \begin{bmatrix} 1 \\ 0 \\ 0 \\ 0 \\ \vdots \\ 0 \end{bmatrix} \quad (2.74)$$

The m_1, m_2, $\cdots$, m_n are the number of processors on the $level_1$, $level_2$, $\cdots$, $level_n$. Also, the α_{l0}, α_{l1}, $\cdots$, α_{ln} are corresponding workload fraction.

2.3 Without Front End Scenario

2.3.1 Regular Mesh

Data Injection on Corner Processor

2*2 Regular Mesh

This subsection concerns the processors without front-end. Because of without front-end, the processors simultaneously receive the data and only start to process it as soon as each processor receives its entire load assignment. We consider the timing diagram for Fig. 2.3, Fig. 2.6, Fig. 2.9 and so on. In addition, we also give the new closed-form matrix equations for the previous user cases.

Also, the rule also plays a dominate role in establish the mathematics model. The timing diagram of Fig. 2.3 is shown:

P_0 starts to process the assigned workload and it starts to transfer the α_1, α_2 and α_3 fraction workload after it totally receive its α_0 task. That is, P_1 and P_2 are idle until the L_1 finish its data injection to P_0.The similar situation happens to P_1 and P_2 and they both starts to transmit the α_3 after they totaly receive the appropriate workload. In other words, P_3 has to wait until the previous two level processors obtains their own data.

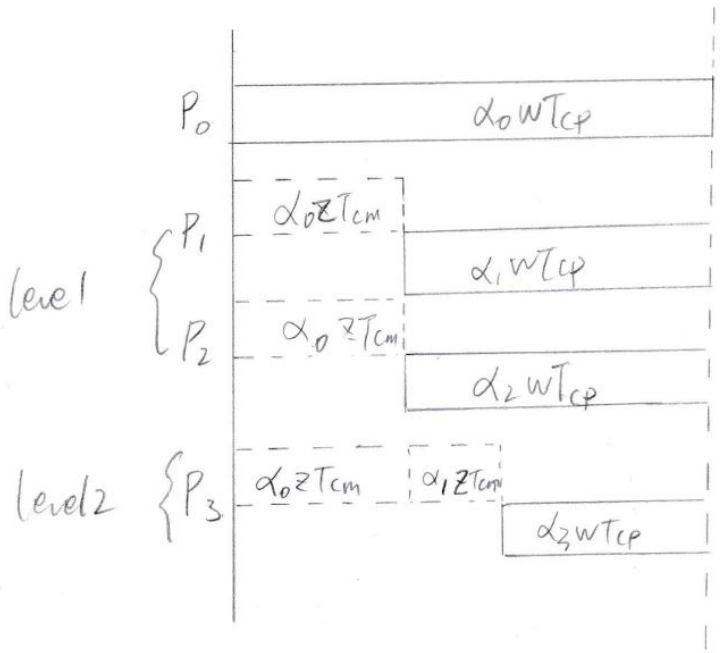

Figure 2.23: The timing diagram for 2*2 regular mesh without front end.

The corresponding group of equations are as follows:

$$\begin{cases} \alpha_0 \omega T_{cp} = T_{f,m} & (2.75) \\ \alpha_1 z T_{cm} + \alpha_1 \omega T_{cp} = T_{f,m} & (2.76) \\ \alpha_2 z T_{cm} + \alpha_2 \omega T_{cp} = T_{f,m} & (2.77) \\ (\alpha_1 + \alpha_3) z T_{cm} + \alpha_3 \omega T_{cp} = T_{f,m} & (2.78) \\ \sigma = \dfrac{z T_{cm}}{\omega T_{cp}} & (2.79) \\ \alpha_0 + \alpha_1 + \alpha_2 + \alpha_3 = 1 & (2.80) \\ 0 < \sigma < 1 & (2.81) \\ 0 < \alpha_0, \alpha_1, \alpha_2, \alpha_3 < 1 & (2.82) \end{cases}$$

The group of equations imply that

$$\alpha_1 = \alpha_2$$

Further, the equations test and verify the rule again.

The matrix closed-from is presented as:

$$\begin{bmatrix} 1 & 2 & 1 \\ 1 & -(\sigma+1) & 0 \\ 1 & -\sigma & -(\sigma+1) \end{bmatrix} \times \begin{bmatrix} \alpha_0 \\ \alpha_1 \\ \alpha_3 \end{bmatrix} = \begin{bmatrix} 1 \\ 0 \\ 0 \end{bmatrix} \tag{2.83}$$

The simulation result for Fig. 2.3 is provided in Fig. 2.24:

Fig. 2.24 explains that as the σ value grows up, the fraction is assigned to P_0 increases and the fraction are distributed to $level_1$ and $level_2$ reduce. In other words, if the communication capability decreases, there are more data processed locally, which is reasonable. If the ability of the link decrease asymptotically equal to the processor computation capacity, there is only 10% data is deployed to the $level_2$. In addition, if the $\sigma > 1$, it means the link transmitting power is less than the processor's processing ability. In this scenario, keeping the data locally is more economical than transmitting it.

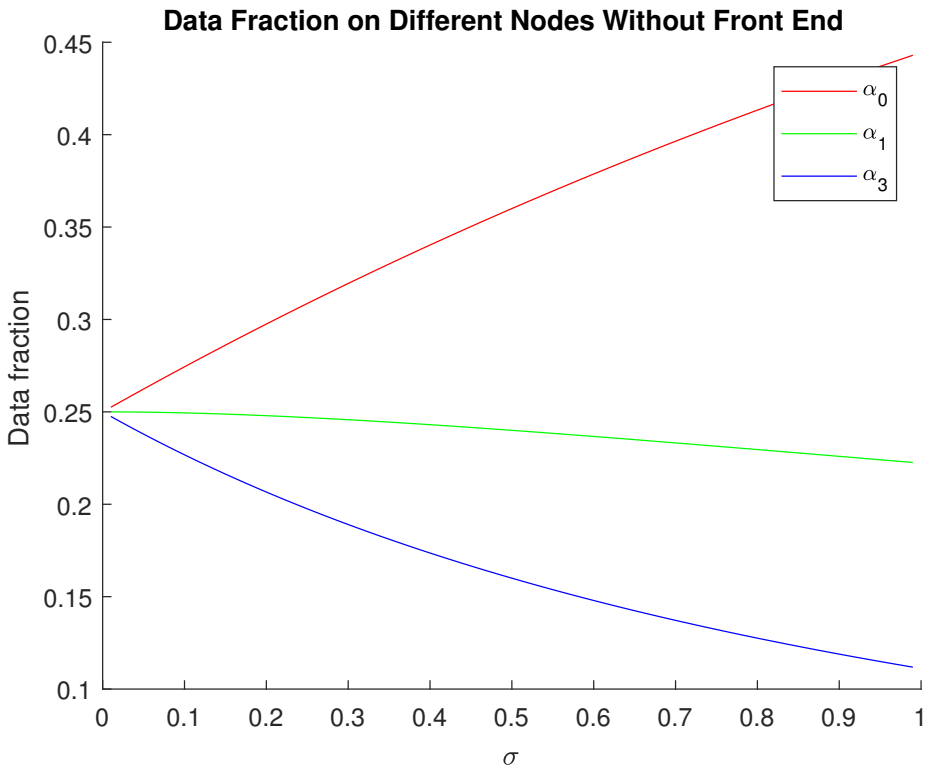

Figure 2.24: The data fraction deployed based on the radius value

2*3 Regular Mesh

P_0 starts to process the assigned workload and it starts to transfer the α_1, α_2 , α_3, α_5, α_5 fraction workload after it totally receive its α_0 task. That is, P_1 and P_2 are idle until the L_1 finish its data injection to P_0.$Accordingtothelevel$1The similar situation happens to P_1 and P_2 and they both starts to transmit the α_3 after they totally receive the appropriate workload. In other words, P_3 has to wait until the previous three levels, $level_0$, $level_1$ and $level_2$ processors obtain their own data.

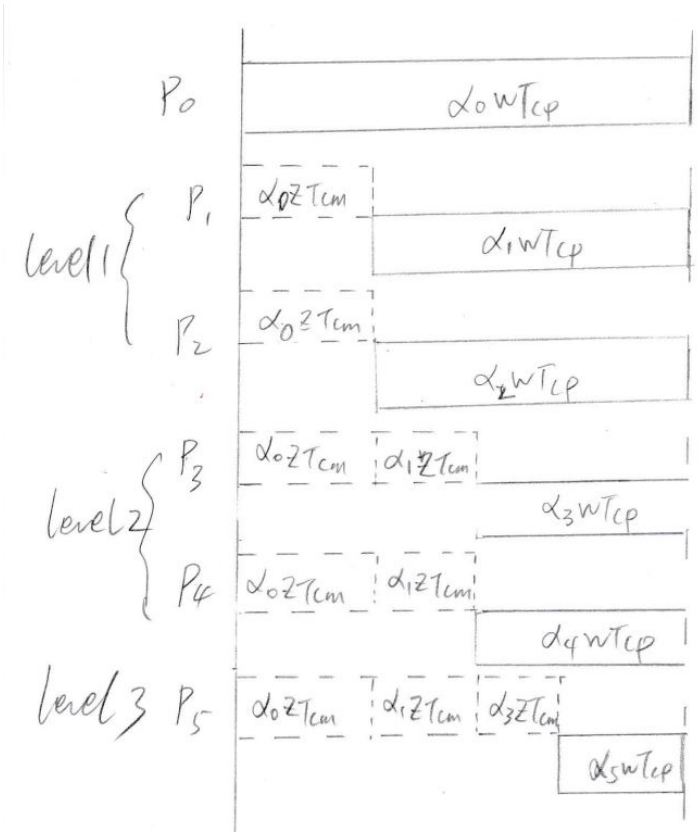

Figure 2.25: The timing diagram for 2*3 regular mesh without front end.

In addition, the group of equations are as follows:

$$\begin{cases} \alpha_0 \omega T_{cp} = T_{f,m} & (2.84) \\ \alpha_1 z T_{cm} + \alpha_1 \omega T_{cp} = T_{f,m} & (2.85) \\ \alpha_2 z T_{cm} + \alpha_2 \omega T_{cp} = T_{f,m} & (2.86) \\ (\alpha_1 + \alpha_3) z T_{cm} + \alpha_3 \omega T_{cp} = T_{f,m} & (2.87) \\ (\alpha_1 + \alpha_4) z T_{cm} + \alpha_4 \omega T_{cp} = T_{f,m} & (2.88) \\ (\alpha_1 + \alpha_3 + \alpha_5) z T_{cm} + \alpha_5 \omega T_{cp} = T_{f,m} & (2.89) \\ \sigma = \dfrac{z T_{cm}}{\omega T_{cp}} & (2.90) \\ \alpha_0 + \alpha_1 + \alpha_2 + \alpha_3 + \alpha_4 + \alpha_5 = 1 & (2.91) \end{cases}$$

$$\begin{bmatrix} 1 & 2 & 2 & 1 \\ 1 & -(\sigma+1) & 0 & 0 \\ 1 & -\sigma & -(\sigma+1) & 0 \\ 1 & -\sigma & -\sigma & -(\sigma+1) \end{bmatrix} \times \begin{bmatrix} \alpha_0 \\ \alpha_1 \\ \alpha_3 \\ \alpha_5 \end{bmatrix} = \begin{bmatrix} 1 \\ 0 \\ 0 \\ 0 \end{bmatrix} \quad (2.92)$$

The speedup is

$$Speedup = \frac{T_{f,0}}{T_{f,n}} = \frac{\omega T_{cp}}{\alpha_0 \omega T_{cp}} = \frac{1}{\alpha_0}$$

The simulation result is:

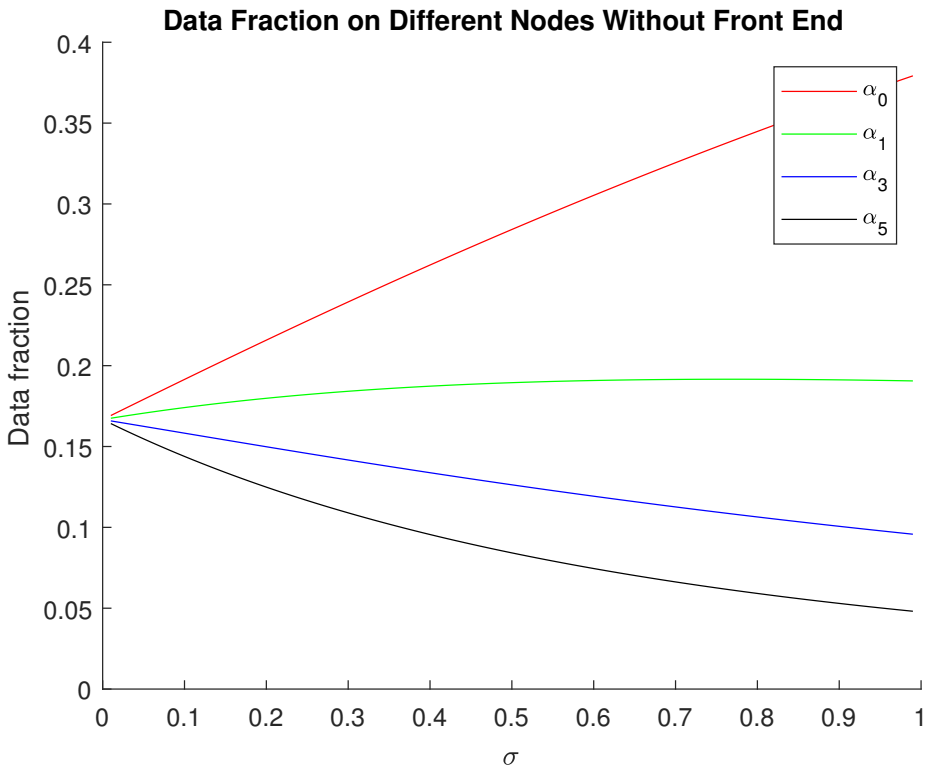

Figure 2.26: The data fraction deployed based on the radius value

2*n Regular Mesh

Considering Fig. 2.9, the equations are demonstrated as follows:

$$
\begin{cases}
\alpha_1 z T_{cm} + \alpha_1 \omega T_{cp} = T_{f,m} & (2.93) \\
\alpha_2 z T_{cm} + \alpha_2 \omega T_{cp} = T_{f,m} & (2.94) \\
(\alpha_1 + \alpha_3) z T_{cm} + \alpha_3 \omega T_{cp} = T_{f,m} & (2.95) \\
(\alpha_1 + \alpha_4) z T_{cm} + \alpha_4 \omega T_{cp} = T_{f,m} & (2.96) \\
(\alpha_1 + \alpha_3 + \alpha_5) z T_{cm} + \alpha_5 \omega T_{cp} = T_{f,m} & (2.97) \\
\vdots & (2.98) \\
(\alpha_1 + \alpha_3 + \cdots + \alpha_{2\times n+1}) z T_{cm} + \alpha_{2\times n-1} \omega T_{cp} = T_{f,m} & (2.99) \\
\sigma = \dfrac{z T_{cm}}{\omega T_{cp}} & (2.100) \\
0 < \sigma < 1 & (2.101) \\
0 < \alpha_0 \quad \alpha_1 \quad \alpha_3 \quad \cdots \quad \alpha_{2\times n-1} < 1 & (2.102)
\end{cases}
$$

The matrix form for the group of equations are:

$$\begin{bmatrix} 1 & 2 & 2 & \cdots & 2 & 2 & 1 \\ 1 & -(\sigma+1) & 0 & \cdots & 0 & 0 & 0 \\ 1 & -\sigma & -(\sigma+1) & \cdots & 0 & 0 & 0 \\ 1 & -\sigma & -\sigma & -(\sigma+1) & 0 & \cdots & 0 \\ 1 & -\sigma & -\sigma & -\sigma & -(\sigma+1) & 0 & 0 \\ \vdots & \vdots & \vdots & \vdots & \ddots & \ddots & \\ 1 & -\sigma & -\sigma & \cdots & -\sigma & -\sigma & -(\sigma+1) \end{bmatrix} \times \begin{bmatrix} \alpha_0 \\ \alpha_1 \\ \alpha_3 \\ \alpha_5 \\ \vdots \\ \alpha_{2\times n-3} \\ \alpha_{2\times n-1} \end{bmatrix} = \begin{bmatrix} 1 \\ 0 \\ 0 \\ 0 \\ \vdots \\ 0 \end{bmatrix} \tag{2.103}$$

m*n Regular Mesh

Referring to Fig. 2.12, we utilize $\sigma^\star$ to present the $-(\sigma+1)$. The matrix closed-form is:

$$\begin{bmatrix} 1 & 2 & 3 & 4 & 5 & 4 & 3 & 2 & 1 \\ 1 & \sigma^\star & 0 & 0 & 0 & 0 & 0 & 0 & 0 \\ 1 & -\sigma & \sigma^\star & 0 & 0 & 0 & 0 & 0 & 0 \\ 1 & -\sigma & -\sigma & \sigma^\star & 0 & 0 & 0 & 0 & 0 \\ 1 & -\sigma & -\sigma & -\sigma & \sigma^\star & 0 & 0 & 0 & 0 \\ 1 & -\sigma & -\sigma & -\sigma & -\sigma & \sigma^\star & 0 & 0 & 0 \\ 1 & -\sigma & -\sigma & -\sigma & -\sigma & -\sigma & \sigma^\star & 0 & 0 \\ 1 & -\sigma & -\sigma & -\sigma & -\sigma & -\sigma & -\sigma & \sigma^\star & 0 \\ 1 & -\sigma & -\sigma & -\sigma & -\sigma & -\sigma & -\sigma & -\sigma & \sigma^\star \end{bmatrix} \times \begin{bmatrix} \alpha_0 \\ \alpha_1 \\ \alpha_3 \\ \alpha_6 \\ \alpha_{10} \\ \alpha_{15} \\ \alpha_{19} \\ \alpha_{22} \\ \alpha_{24} \end{bmatrix} = \begin{bmatrix} 1 \\ 0 \\ 0 \\ 0 \\ 0 \\ 0 \\ 0 \\ 0 \\ 0 \end{bmatrix} \tag{2.104}$$

Data Injection on Boundary Processor

Fig. 2.13 shows an example of boundary processor P_0 receiving the L_1 The timing diagram for Fig. 2.13 is Fig. 2.27.

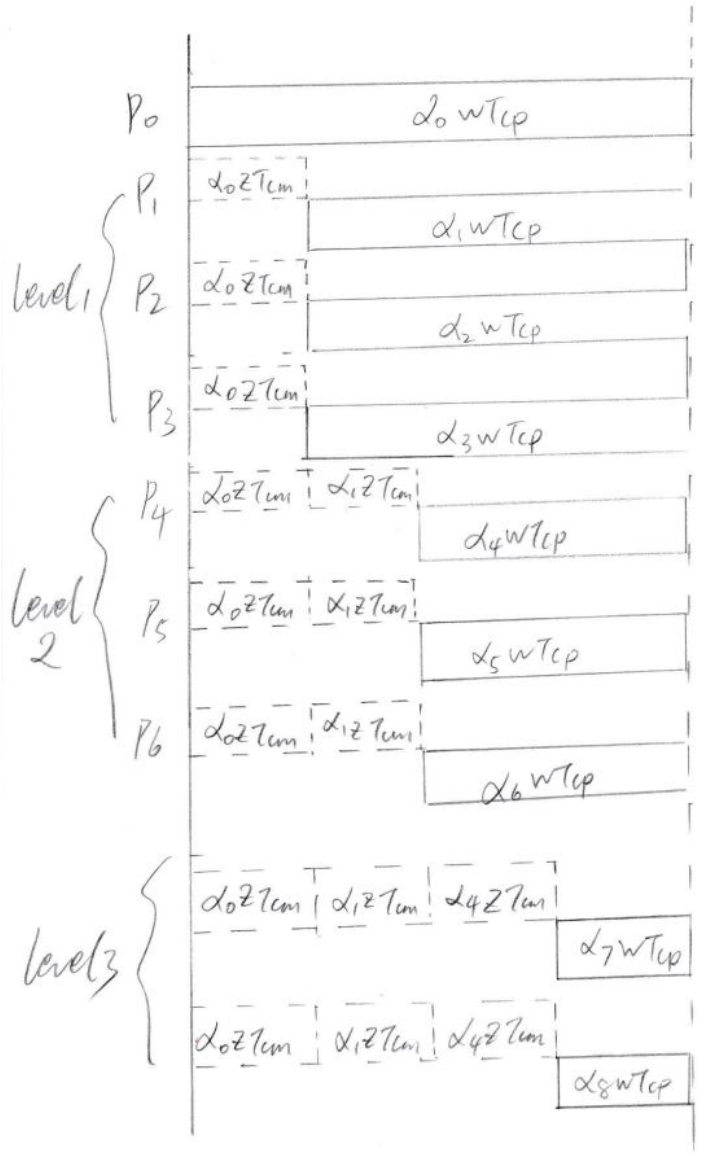

Figure 2.27: The timing diagram for 3*3 boundary data injection on P_0

$$
\begin{cases}
\alpha_0 \omega T_{cp} = T_{f,m} & (2.105) \\
\alpha_1 z T_{cm} + \alpha_1 \omega T_{cp} = T_{f,m} & (2.106) \\
\alpha_2 z T_{cm} + \alpha_2 \omega T_{cp} = T_{f,m} & (2.107) \\
\alpha_3 z T_{cm} + \alpha_3 \omega T_{cp} = T_{f,m} & (2.108) \\
(\alpha_1 + \alpha_4) z T_{cm} + \alpha_4 \omega T_{cp} = T_{f,m} & (2.109) \\
(\alpha_2 + \alpha_5) z T_{cm} + \alpha_5 \omega T_{cp} = T_{f,m} & (2.110) \\
(\alpha_3 + \alpha_6) z T_{cm} + \alpha_6 \omega T_{cp} = T_{f,m} & (2.111) \\
(\alpha_1 + \alpha_4 + \alpha_7) z T_{cm} + \alpha_7 \omega T_{cp} = T_{f,m} & (2.112) \\
(\alpha_1 + \alpha_4 + \alpha_8) z T_{cm} + \alpha_8 \omega T_{cp} = T_{f,m} & (2.113) \\
\sigma = \dfrac{z T_{cm}}{\omega T_{cp}} & (2.114) \\
0 < \sigma < 1 & (2.115) \\
0 < \alpha_0 \quad \alpha_1 \quad \alpha_3 \quad \alpha_4 \quad \alpha_5 \quad \alpha_6 \quad \alpha_7 \quad \alpha_8 < 1 & (2.116)
\end{cases}
$$

$$
\begin{bmatrix}
1 & 3 & 3 & 2 \\
1 & -(\sigma+1) & 0 & 0 \\
1 & -\sigma & -(\sigma+1) & 0 \\
1 & -\sigma & -\sigma & -(\sigma+1)
\end{bmatrix}
\times
\begin{bmatrix}
\alpha_0 \\ \alpha_1 \\ \alpha_4 \\ \alpha_7
\end{bmatrix}
=
\begin{bmatrix}
1 \\ 0 \\ 0 \\ 0
\end{bmatrix}
\qquad (2.117)
$$

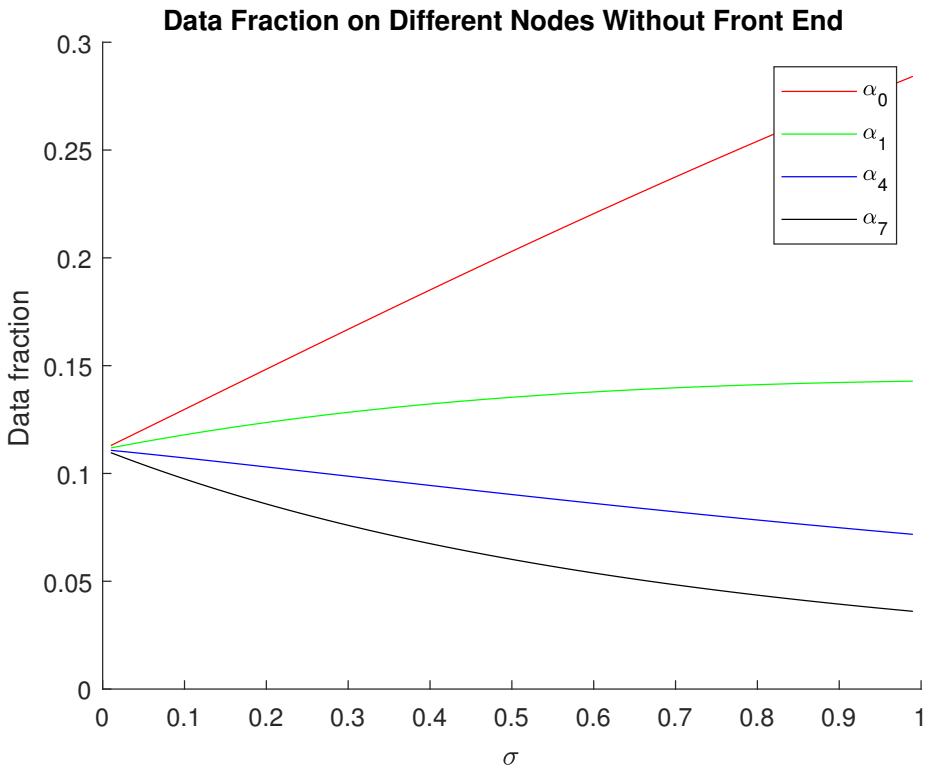

Figure 2.28: The fraction curve for 3*3 boundary data injection on P_0

Data Injection on The Inner Grid Processor

The equations are:

$$
\begin{cases}
\alpha_0 \omega T_{cp} = T_{f,m} & (2.118) \\
\alpha_1 z T_{cm} + \alpha_1 \omega T_{cp} = T_{f,m} & (2.119) \\
\alpha_2 z T_{cm} + \alpha_2 \omega T_{cp} = T_{f,m} & (2.120) \\
\alpha_3 z T_{cm} + \alpha_3 \omega T_{cp} = T_{f,m} & (2.121) \\
\alpha_4 z T_{cm} + \alpha_4 \omega T_{cp} = T_{f,m} & (2.122) \\
(\alpha_1 + \alpha_5) z T_{cm} + \alpha_5 \omega T_{cp} = T_{f,m} & (2.123) \\
(\alpha_2 + \alpha_6) z T_{cm} + \alpha_6 \omega T_{cp} = T_{f,m} & (2.124) \\
(\alpha_3 + \alpha_7) z T_{cm} + \alpha_7 \omega T_{cp} = T_{f,m} & (2.125) \\
(\alpha_4 + \alpha_8) z T_{cm} + \alpha_8 \omega T_{cp} = T_{f,m} & (2.126) \\
\sigma = \dfrac{z T_{cm}}{\omega T_{cp}} & (2.127) \\
0 < \sigma < 1 & (2.128) \\
0 < \alpha_0 \quad \alpha_1 \quad \alpha_3 \quad \alpha_4 \quad \alpha_5 \quad \alpha_6 \quad \alpha_7 \quad \alpha_8 < 1 & (2.129)
\end{cases}
$$

The matrix closed-form is:

$$
\begin{bmatrix}
1 & 4 & 4 \\
1 & -(\sigma+1) & 0 \\
1 & -\sigma & -(\sigma+1)
\end{bmatrix}
\times
\begin{bmatrix}
\alpha_0 \\ \alpha_1 \\ \alpha_5
\end{bmatrix}
=
\begin{bmatrix}
1 \\ 0 \\ 0
\end{bmatrix}
\tag{2.130}
$$

The simulation result shows:

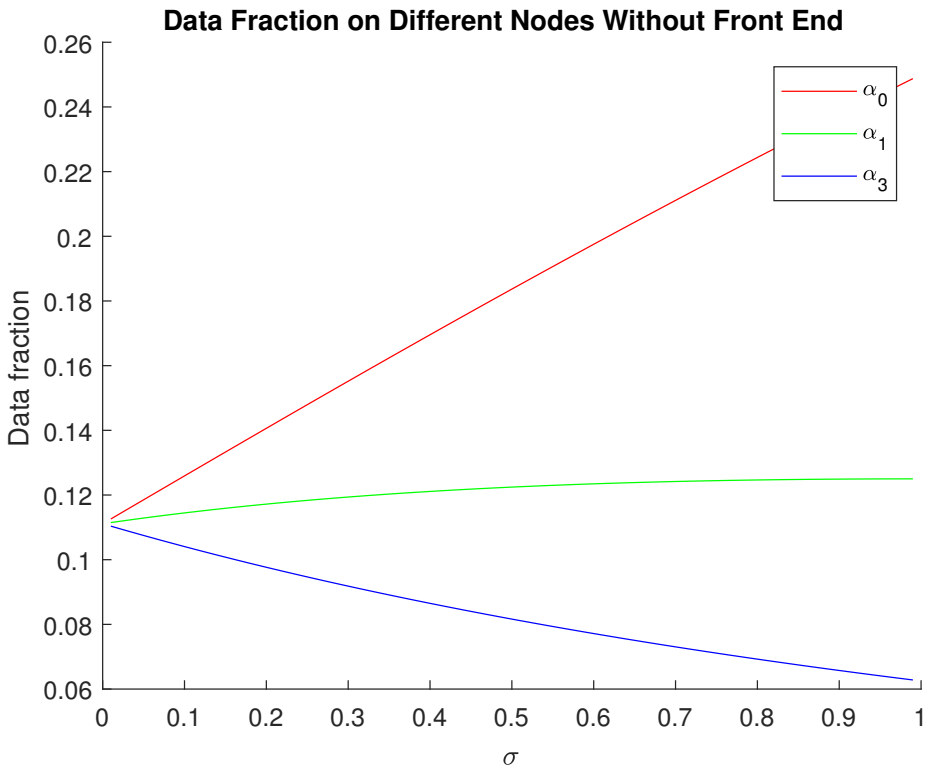

Figure 2.29: The timing diagram for 3*3 inner grid injection P_0

2.3.2 Toroidal Mesh

We utilize the $\sigma^\star$ to present $-(\sigma+1)$. The matrix closed-form is:

$$\begin{bmatrix} 1 & 4 & 8 & 10 & 8 & 4 & 1 \\ 1 & \sigma^{\star} & 0 & 0 & 0 & 0 & 0 \\ 1 & -\sigma & \sigma^{\star} & 0 & 0 & 0 & 0 \\ 1 & -\sigma & -\sigma & -\sigma^{\star} & 0 & 0 & 0 \\ 1 & -\sigma & -\sigma & -\sigma & \sigma^{\star} & 0 & 0 \\ 1 & -\sigma & -\sigma & -\sigma & -\sigma & \sigma^{\star} & 0 \\ 1 & -\sigma & -\sigma & -\sigma & -\sigma & sigma & \sigma^{\star} \end{bmatrix} \times \begin{bmatrix} \alpha_0 \\ \alpha_1 \\ \alpha_2 \\ \alpha_3 \\ \alpha_4 \\ \alpha_5 \\ \alpha_6 \end{bmatrix} = \begin{bmatrix} 1 \\ 0 \\ 0 \\ 0 \\ 0 \\ 0 \\ 0 \end{bmatrix} \tag{2.131}$$

The simulation result is :

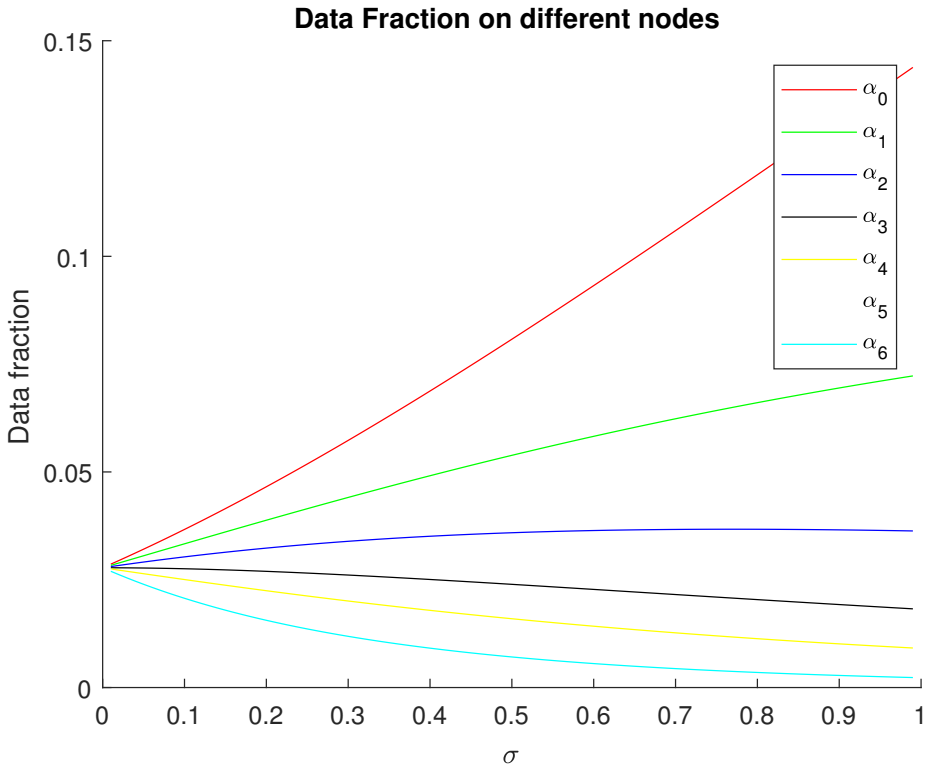

Figure 2.30: The data fraction deployed based on the radius value

2.3.3 General Case

$$\begin{bmatrix} 1 & m_1 & m_2 & \cdots & m_{n-2} & m_{n-1} & m_n \\ 1 & -(\sigma+1) & 0 & \cdots & 0 & 0 & 0 \\ 1 & -\sigma & -(\sigma+1) & \cdots & 0 & 0 & 0 \\ 1 & -\sigma & -\sigma & -(\sigma+1) & 0 & \cdots & 0 \\ 1 & -\sigma & -\sigma & -\sigma & -(\sigma+1) & 0 & 0 \\ \vdots & \vdots & \vdots & \vdots & \ddots & \ddots & \\ 1 & -\sigma & -\sigma & \cdots & -\sigma & -\sigma & -(\sigma+1) \end{bmatrix} \times \begin{bmatrix} \alpha_{l_0} \\ \alpha_{l_1} \\ \alpha_{l_2} \\ \alpha_{l_3} \\ \vdots \\ \alpha_{l_{n-1}} \\ \alpha_{l_n} \end{bmatrix} = \begin{bmatrix} 1 \\ 0 \\ 0 \\ 0 \\ \vdots \\ 0 \end{bmatrix} \tag{2.132}$$

The m_1, m_2, $\cdots$, m_n are the number of processors on the $level_1$, $level_2$, $\cdots$, $level_n$. Also, the α_{l0}, α_{l1}, $\cdots$, α_{ln} are corresponding workload fraction.

2.4 Comparing Result Between Front End Processor and Without Front End Processor

In the legend of figures, we use F to present the front-end situation and use NF to presents the without front-end processors setting, for example $F\alpha_0$ means the α_0 data fraction deployed to P_0, if the processor has front-end. $NF\alpha_0$ means the α_0 data fraction deployed to P_0, if the processor is without front-end setting.

2.4.1 Regular Mesh

On the Corner Processor

Fig. 2.31 says that P_0 takes more assigned task in without front-end scenario than front-end processor situation. As the σ value goes up, the fractions are deployed to the deeper levels dropping down. In the limit condition, for example, $\sigma = 1$, there is no data transmitted to P_3 in the front-end assumption, yet in the without front-end situation, there is still about 10% data fraction are communicated to P_3.

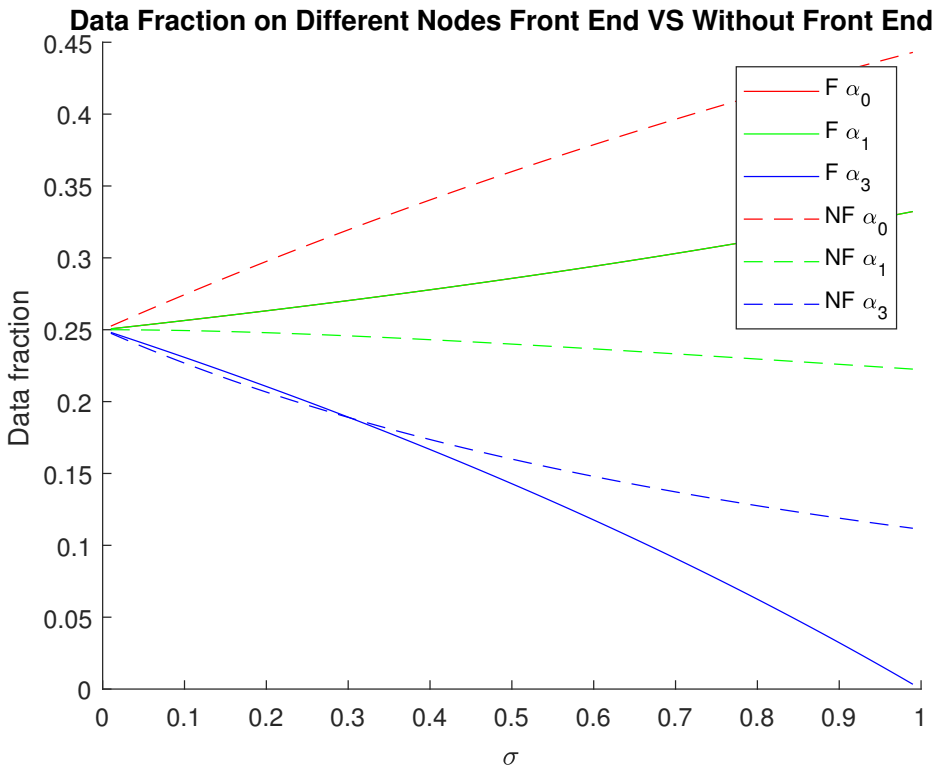

Figure 2.31: The comparing result between front-end processor with without front-end processor in 2*2 regular mesh

Fig. 2.32 says that P_0 takes more assigned task in without front-end scenario than front-end processor situation. As the σ value goes up, the fractions are deployed to the deeper levels dropping down. In the limit condition, for example, $\sigma = 1$, there is no data transmitted to $level_3$, that is, P_5 in the front-end assumption. Yet in the without front-end situation, there is still about 5% data fraction is communicated to P_5.

Fig. 2.33 says that P_0 takes more assigned task in without front-end scenario than front-end processor situation. As the σ value goes up, the fractions

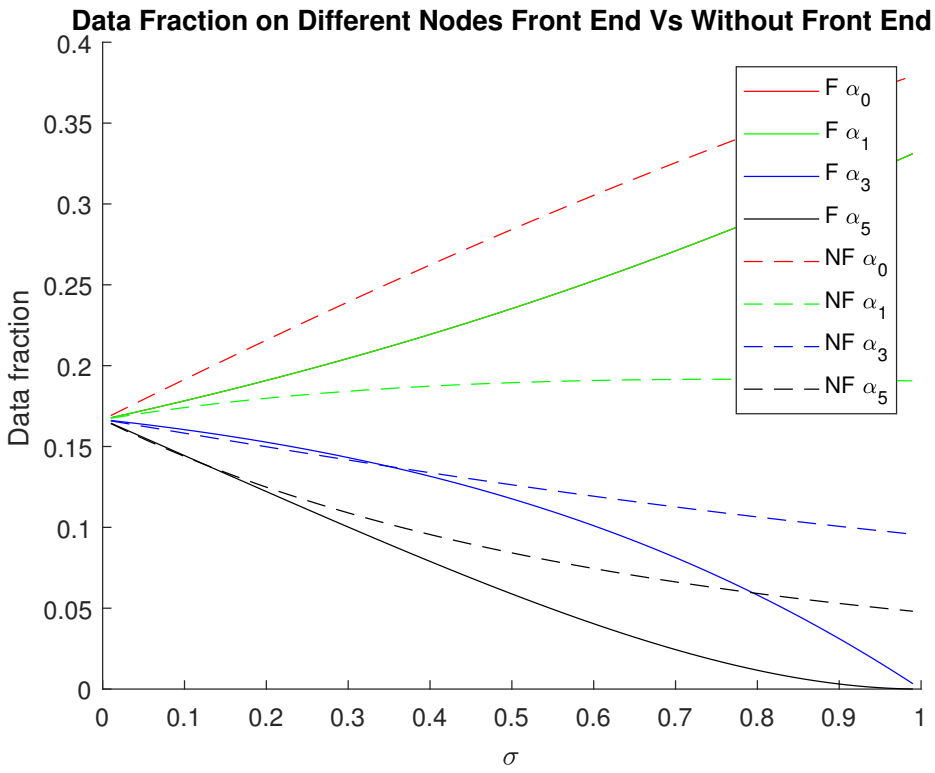

Figure 2.32: The comparing result between front-end processor with without front-end processor in 2*4 regular mesh

are deployed to the deeper levels dropping down. In the limit condition, for example, $\sigma = 1$, there is no data transmitted to $level_3$, that is, P_7 and P_8 in the front-end assumption. Yet in the without front-end situation, there is still about 5% data fraction is communicated to P_7 and P_8.

Fig. 2.34 says that P_0 takes more assigned task in without front-end scenario than front-end processor situation. As the σ value goes up, the fractions are deployed to the deeper levels dropping down. In the limit condition, for example, $\sigma = 1$, there is no data transmitted to $level_2$, that is, P_5, P_6, P_7 and

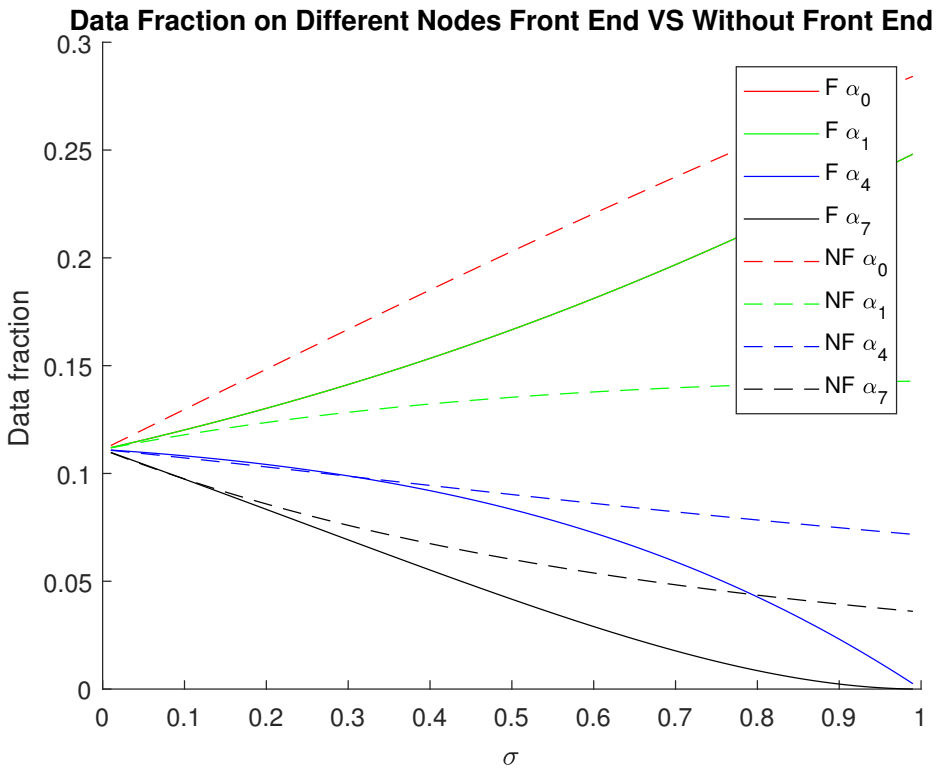

Figure 2.33: The comparing result between front-end processor with without front-end processor in 3*3 regular mesh injection on boundary processor

P_8 in the front-end assumption. Yet in the without front-end situation, there is still about 5% data fraction is communicated to P_5, P_6, P_7 and P_8.

Comparing with Fig. 2.33, P_0 takes less workload in inner grid position than boundary data injection. The reason is there are 4 neighbor processors on the $level_1$, yet there is only three processors on $level_1$ in boundary plan. In other words, the $level_1$ plays a critical role in data deployed.

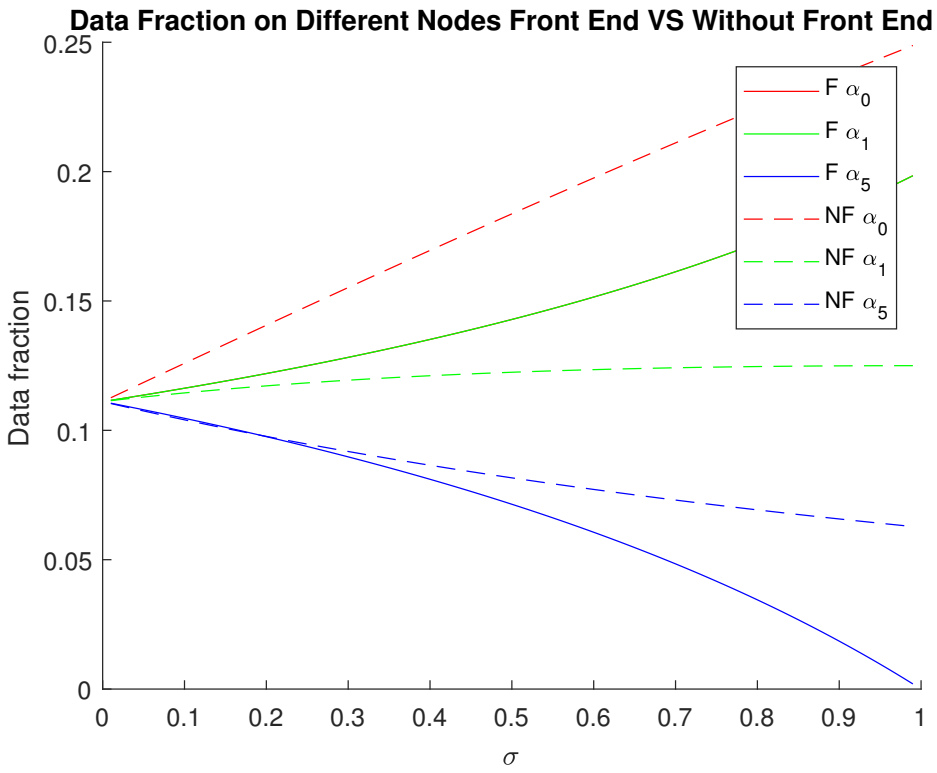

Figure 2.34: The comparing result between front-end processor with without front-end processor in 3*3 regular mesh injection on inner grid processor

2.4.2 Toroidal

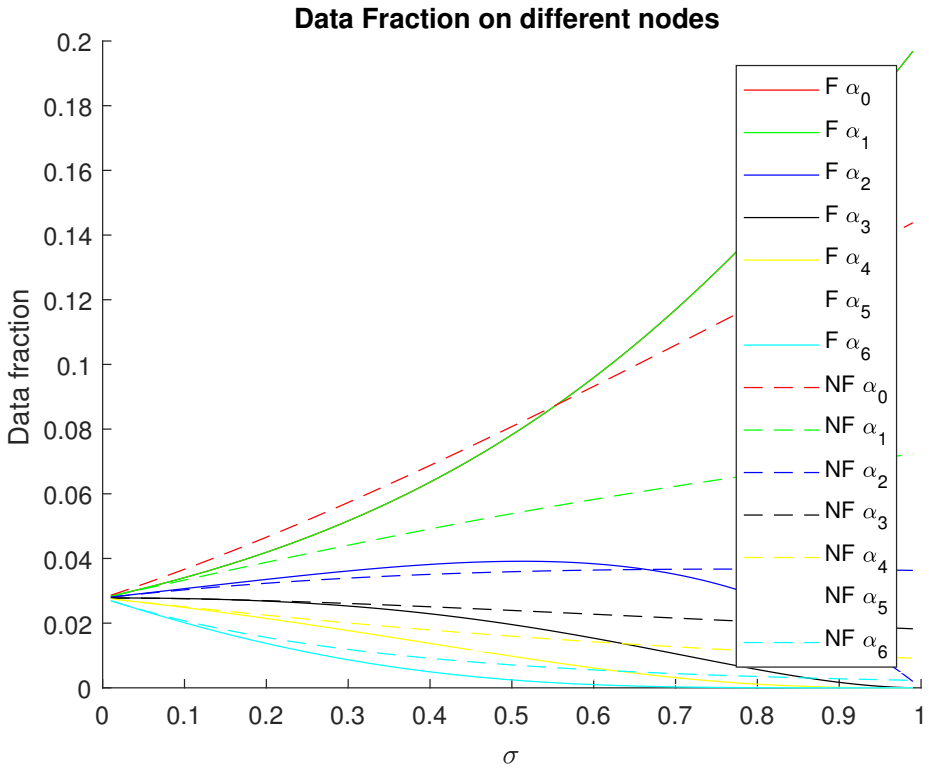

Figure 2.35: The comparing result between front-end processor with without front-end processor in 6*6 regular mesh injection on inner grid processor

Chapter 3

Sensitivity Analysis

Chapter 4

Multi-source Assignment Utilizing Voronoi Diagram

Chapter 5

Multi-source Re-assignment Using Optimal Mass Transportation

Chapter 6

Conclusions

Bibliography

[1] M. Moges, D. Yu, and T. G. Robertazzi, "Grid scheduling divisible loads from two sources," *Computers & Mathematics with Applications*, vol. 58, no. 6, pp. 1081–1092, 2009.

[2] T. G. Robertazzi, "Processor equivalence for daisy chain load sharing processors," *IEEE Transactions on Aerospace and Electronic Systems*, vol. 29, no. 4, pp. 1216–1221, 1993.

[3] X. Liu, H. Zhao, and X. Li, "1scheduling divisible workloads from multiple sources in linear daisy chain networks."

[4] C. F. Gamboa and T. Robertazzi, "Simple performance bounds for multicore and parallel channel systems," *Parallel Processing Letters*, vol. 21, no. 04, pp. 439–460, 2011.

[5] V. Bharadwaj, *Scheduling divisible loads in parallel and distributed systems*, vol. 8. John Wiley & Sons, 1996.

[6] J. T. Hung and T. G. Robertazzi, "Switching in sequential tree networks," *IEEE Transactions on Aerospace and Electronic Systems*, vol. 40, no. 3, pp. 968–982, 2004.

[7] V. Bharadwaj, D. Ghose, and T. G. Robertazzi, "Divisible load theory: A new paradigm for load scheduling in distributed systems," *Cluster Computing*, vol. 6, no. 1, pp. 7–17, 2003.

[8] T. G. Robertazzi, "Toroidal networks," *IEEE Communications Magazine*, vol. 26, no. 6, pp. 45–50, 1988.